Mission Definition Document

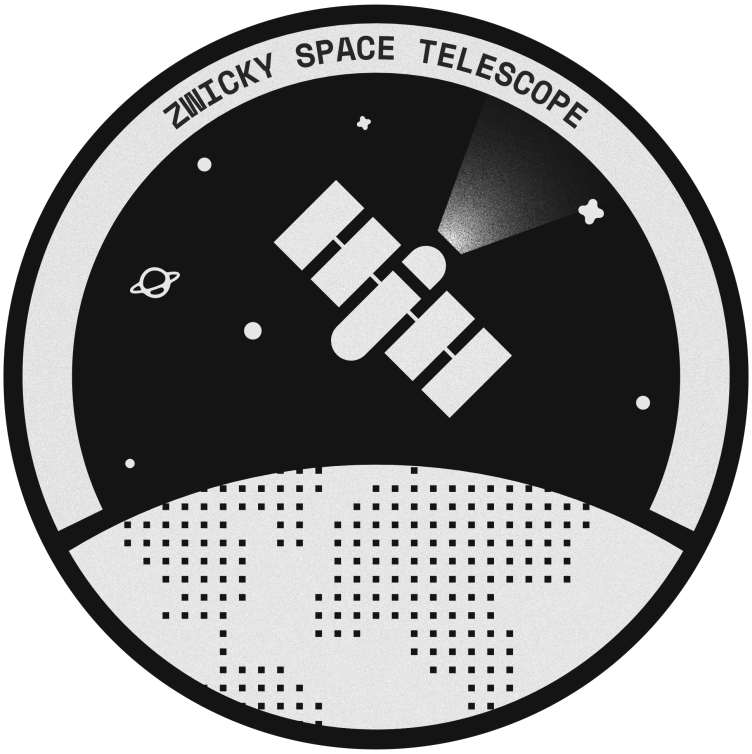

Zwicky Space Telescope

G. Ardito, A. Collogrosso, F. Cuzzocrea, B. Lui,
P. Pansini, M. L. Tramis, A. Turano, E. P. Viviani

Issue: 1
Document type: MDD

" The universe is so unique and perfect that it could not have originated by chance but was divined by flawless, creative design "

Fritz Zwicky

Contents

1 General information related to the context of the document **1**
1.1 Scope of the document . . . 1
1.2 Abbreviated Terms . . . 1
1.3 Reference Books . . . 3
1.4 Reference Articles . . . 4
1.5 Applicable Documents . . . 4
1.6 Datasheets & User Manuals . . . 5

2 Concept Description **6**
2.1 Mission Analysis . . . 6
2.1.1 Mission Information . . . 8
2.1.2 Orbit Related Aspects . . . 8
2.1.3 Environment Description . . . 11
2.2 Overview of the Concept . . . 17
2.2.1 Optical Architecture . . . 19
2.2.2 Optical Design Process . . . 23
2.2.3 Dichroic filter . . . 30
2.2.4 Visible Detector: CCD . . . 33
2.2.5 NIR detector: Spectrometer architecture . . . 39
2.2.6 Data Compression . . . 47
2.2.7 On-board data handling architecture . . . 50
2.2.8 Power Bus . . . 51
2.3 System Description . . . 53
2.3.1 Launch Vehicle . . . 53
2.3.2 Spacecraft . . . 56
2.3.3 Structures . . . 56
2.3.4 CCD Unit . . . 61
2.3.5 Spectrometer . . . 61
2.3.6 Payload Data Handling . . . 62
2.3.7 Power Control and Distribution Unit . . . 65
2.3.8 Thermal Control Subsystem . . . 66
2.3.9 Components Shielding . . . 69
2.4 Description of how the system works in each mission phase . . . 70
2.4.1 Mission Phases Description . . . 70
2.4.2 Technology Readiness Level . . . 71

2.4.3 Operative Modes 72

3 Assessment of the performances **74**
3.1 Mass Budget 74
3.2 Power Budget 75
3.3 Data Budget 75

4 Identification of risk areas **78**
4.1 Optics 78
4.2 CCD Array 78
4.3 Spectrometer Array 78
4.4 Structure 79
4.5 Thermal Control Subsystem 79
4.6 Payload Data Handling Subsystem 79

5 Conclusions **80**

Chapter 1

General information related to the context of the document

1.1 Scope of the document

This document defines the purposes, explains the objectives of the product and provides a possible concept of the mission specifications that could satisfy the preliminary technical requirements specification (TS).
The document provides a complete description of the concept, considering performance drivers, constraints, main events and operational scenarios.

1.2 Abbreviated Terms

ADCS Attitude Determination and Control Subsystem

ASIC Application Specific Integrated Circuit

C.R. Compression Ratio

CCD Charge Couple Device

CCSDS Consultative Committee for Space Data Systems

CMOS Complementary Metal-Oxide Semiconductor

CPU Central Processing Unit

CWICOM CCSDS Wavelet Image COMpression ASIC

DPU Data Processing Unit

DSO Deep Space Object

DWT Discrete Wavelet Transform

ECC Error Correction Code

ECSS European Cooperation for Space Standardization

EEPROM Electrically Erasable Programmable Read-Only Memory

EOL End of Life

FOV Field of View

FPGA Field Programmable Gate Array

GCR Galactic Cosmic Ray

GS Ground Station

HEO Highly Elliptical Orbit

HW Hardware

I/O Input/Output

I2C Inter Integrated Circuit

KO Knight Optics

LET Linear Energy Transfer

LVDS Low-voltage differential signaling

LWP Long Wave Pass

MLI Multy-Layer Insulator

NIR Near Infrared Radiation

OBC On-Board Computer

OBDH On Board Data Handling

OS Operating System

PC Personal Computer

PCI Peripheral Component Interconnect

PCU Power Control Unit

PDHS Payload Data Handling Subsystem

PRDC Payload Rice Data Compressor

QE Quantum Efficiency

S/C Spacecraft

SEU Single Event Upset

SNR Signal-to-Noise Ratio

SOC System-on-Chip

SPI Serial Peripheral Interface

SPU Science Processing Unit

SRAM Static Random Access Memory

SRP Solar Radiation Pressure

SW Software

SWP Short Wave Pass

TBD To Be Defined

TCS Thermal Control Subsystem

TID Total Ionizing Dose

TRL Technology Readiness Level

VIS Visible Spectrum

1.3 Reference Books

[1] Pierre Y. Bely
The design and construction of large optical telescopes

[2] Jingquan Cheng
The Principles of Astronomical Telescope Design.

[3] Lee Feinberg, Lester Cohen, Bruce Dean, William Hayden, Joseph Howard, Ritva Keski-Kuha
Space telescope design considerations.

[4] Mark R. Ackemann; John T. McGraw; Peter C. Zimmer
An Overview of Wide-Field-Of-View Optical Designs for Survey Telescopes.

[5] Pierre-Yves Bely; Christopher J. Burrows; Garth D. Illingworth
The Next Generation Space Telescope.

[6] Charles A. DiMarzio
OPTICS for Engineers.

[7] Dennis Dolkens
A Deployable Telescope for Sub-Meter Resolutions from MicroSatellite Platforms.

[8] Karl Dieter Möller
Optics, Learning by Computing, with Model Examples Using MathCad, MATLAB, Mathematica, and Maple.

[9] Mohamed M. Abid
Spacecraft Sensors.

[10] A.M. Cruise; T.J. Patrick; J.A. Bowles; C.V. Goodall
Principles of space instruments design.

[11] George O. Abell
Abell Galaxy Clusters Catalogue.

[12] Murray Cragin, Emil Bonanno
Uranometria 2000.0 Volume 3, Deep Sky Field Guide.

1.4 Reference Articles

[13] William R. Arnold Sr.; H. Philip Stahl
Structural design consideration for an 8-m space telescope.

[14] Tongtong Wang; Jinsong Gao; Xiaoyi Wang; Hong Chen; Xuanming Zheng
Surface modification on a silicon carbide mirror for space application.

[15] Anna Maria Di Giorgio; Paolo Bastia; Scige J. Liu; Giovanni Giusi; Roberto Scaramella; Mark Cropper; Richard Cole; Ady James; Jérôme Amiaux; Yannick Mellier.
The Command and Data processing Unit of the Euclid Visible Imager:impact of the data compression needs on the unit design.

[16] Rice, Robert E; Pen-Shu Yeh ; Warner H. Miller.
Algorithms for High-speed Universal Noiseless Coding.

[17] Pen-Shu Yeh; Warner H. Miller.
A Real Time Lossless Data Compression Technology for Remote-Sensing and Other Applications.

[18] Pen-Shu Yeh; Warner H. Miller.
Application Guide for Universal Source Coding for Space.

[19] B. Giraud ; J. Vaillant.
CCD Reliabity And Failure Mechanisms Study.

[20] Ibsen photonics
Spectrometer Design Guide

1.5 Applicable Documents

[21] *TS-Zwicky-I1 Rev.0 Zwicky technical requirements specification*, 28 May 2018.

[22] *CCSDS 120.0-G-3 Lossless Data Compression, Green Book*, April 2017.

[23] *CCSDS 122.0-B-2 Image Data Compression, Blue Book*, September 2017.

[24] *ECSS-E-ST-32-08C-Rev.1, Space engineering, materials*, 15 October 2014.

[25] *ECSS-E-ST-10-06C6, Technical requirements specification*, 14 March 2009.

[26] *ECSS-E-ST-10-04C, Space environment*, 31 July 2008.

1.6 Datasheets & User Manuals

[27] www.magellan.aero
Power Control Unit Datasheet

[28] www.esa.int
CWICOM Datasheet

[29] www.baesystems.com
RAD5545 SpaceVPX Datasheet

[30] www.baesystems.com
RAD5510 SpaceVPX Datasheet

[31] www.microchip.com
MG1RT Datasheet

[32] www.microchip.com
AVR ATMegaS128 Datasheet

[33] www.microchip.com
ATMEL ATC18RHA Datasheet

[34] www.e2v.com
CCD231-84 Datasheet

[35] *Ariane 5 User's Manual*

[36] *Ariane 6 User's Manual*

Chapter 2

Concept Description

2.1 Mission Analysis

The aim of Zwicky Space Telescope, from now Zwicky, in memory of the first Dark Matter theorist Fritz Zwicky, is to improve the knowledge of Dark matter and Dark energy through distant galaxy observations. These kind of matter and energy cannot be directly detected, but their effect can be appreciated due to their gravitational interactions.
In particular dark matter contributes to the total gravitational field of galaxies and clusters, which can be measured observing the deflection of light and velocities of nearby particles.
Dark energy, instead, is an anti-gravitational energy theorized to justify the expansion of the universe in continuous acceleration; it is supposed to be smoothly distributed and to affect the geometry of space-time.
There are three main phenomena that can be directly linked as direct consequence of Dark Matter and Dark Energy's presence:

- Weak gravitational lensing
- Galaxies' angular rotation
- Distant galaxy clusters acceleration

Gravitational Lensing is a phenomenon that arises from the distortion of the light coming from a source behind a very massive object like a galaxy. What usually happens is that the huge distortion of the light is not justified just by the visible mass present in front of the light source; in order to fill up this gap, the presence of an undetectable type of mass called "dark matter" has been theorized. In order to study this phenomenon, Zwicky shall be able to acquire and provide images of far galaxies in visible spectrum.
The study of the angular rotation of galaxies is linked to the dark matter in a way similar to the previous phenomenon. According to gravitational theory, the stars which are far from the center of a galaxy should have a lower orbiting velocity compared to the nearer stars. However it has been noticed that near and far stars move almost with the same orbiting velocity, and this can be justified theorizing the presence of more mass around the far stars than what can be detected.
The study of galaxy clusters' acceleration, instead, is linked with the theory of the Dark Energy.

According to physical theories, galaxies are supposed to collapse in one point of the universe because of the gravitational attraction; what inexplicably happens is that galaxies tend to accelerate more and more, moving away one from each other, expanding the universe dimensions. To justify this phenomenon the dark energy has been theorized as an unknown anti-gravitational form of energy that let the galaxy expand at an accelerating rate.
In order to provide data on the galaxies angular rotation and on galaxy clusters velocity, exploiting the Doppler effect, an optical sensor capable to collect both visible and infrared radiation has been chosen.
Two main detectors have been selected to achieve the aim of the mission:

- a Charge Couple Device (CCD) Detector that shall acquire images in the visible spectrum.
- a spectrometer that shall acquire data in the Near-Infrared spectrum.

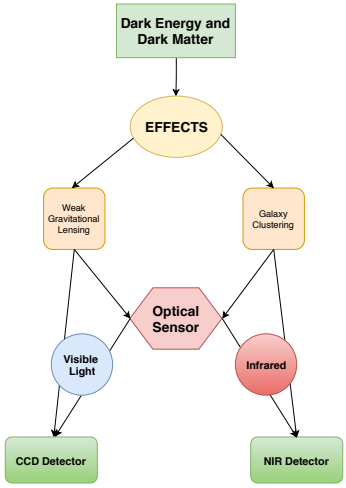

Figure 2.1: Science Flowchart

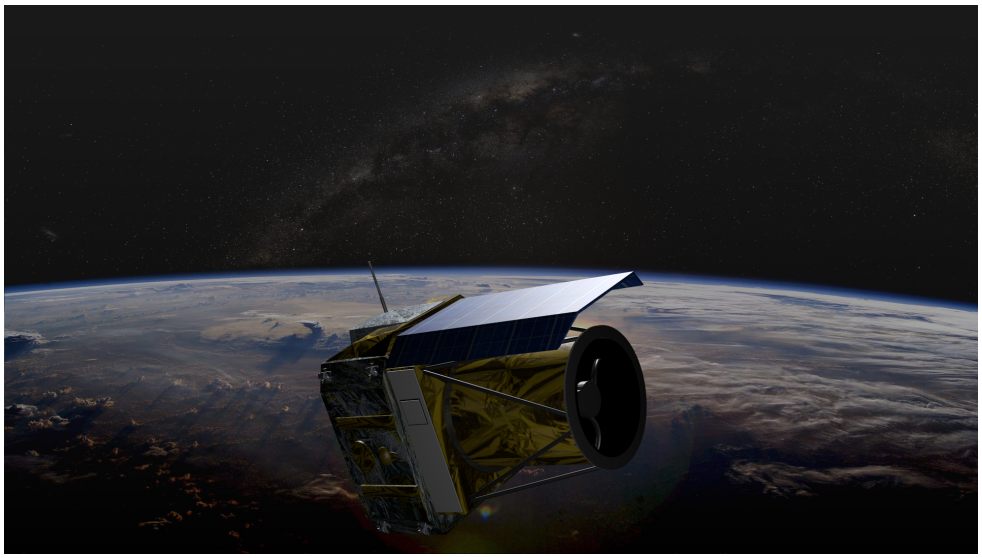

Figure 2.2: Artist's impression of the Zwicky space telescope

2.1.1 Mission Information

Zwicky is the only payload on board and is expected to be launched in 2025, depending on the launch window selected considering stakeholders needs. The Ariane 6 A64 is the selected launcher; a 7 years life cycle has been estimated in order to allow a complete survey of the interested region of space.

2.1.2 Orbit Related Aspects

The S/C will be placed on a highly elliptical orbit (HEO) around Earth with a perigee altitude of 15 000 km and an apogee altitude of 150 000 km (fig. 2.3); the orbit will have a period of ~ 73 hours and its orbital parameters are reported in table 2.1. The HEO orbit has been chosen in order to maximize the time spent near the apogee, because in that region Zwicky shall acquire images. Moreover the HEO orbits are relatively less demanding in terms of energy. When the S/C is in the apogee zone, defined on the orbit by an angle of $\pm 30°$ from the apogee, Zwicky acquires images; the data obtained are then processed and stored on board till the S/C reaches the perigee zone, defined by an angle of $\pm 80°$ from the perigee. It is expected that in this part of orbit that data will be transmitted to the ground by the S/C after a proper compression.
The amount of time estimated for taking images is computed starting from the angular amplitude of the zone and from parameters of the orbit through the following procedure:

Firstly the Eccentric Anomaly is computed for the two angular limits of the zone:

$$\tan\left(\frac{\theta}{2}\right) = \sqrt{\frac{1+e}{1-e}} \cdot \tan\left(\frac{E}{2}\right)$$

Then the time needed to reach that point of the orbit starting from the perigee has been computed:

$$t = \sqrt{\frac{a^3}{\mu}}(E - e \cdot \sin E)$$

At the end the Δt spent in the zone has been computed, considering a difference between times:

$$\begin{aligned} \Delta t &= t_{\theta_2} - t_{\theta_1} && \text{for the apogee zone} \\ \Delta t &= t_{\theta_1} + (T - t_{\theta_2}) && \text{for the perigee zone} \end{aligned}$$

The estimated amount of time for obtaining images and for downloading data are respectively around 46 hours and 4 hours.

Orbital Parameters	
h_a	150000 km
h_p	15000 km
a	88871 km
e	$0,7595$
i	$63,7°$
Ω	$0°$
ω	$0°$
μ	$398600\frac{km^3}{s^2}$
T	$73,2401$ h
$\Delta t_{\text{apogee zone}}$	$46,0705$ h
$\Delta t_{\text{perigee zone}}$	$4,0035$ h

Table 2.1: Parameters of the operative orbit

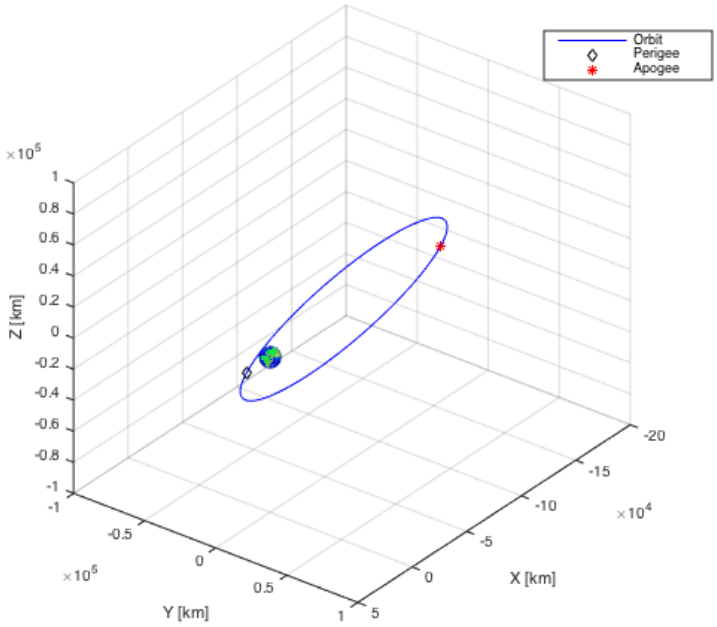

Figure 2.3: Orbit

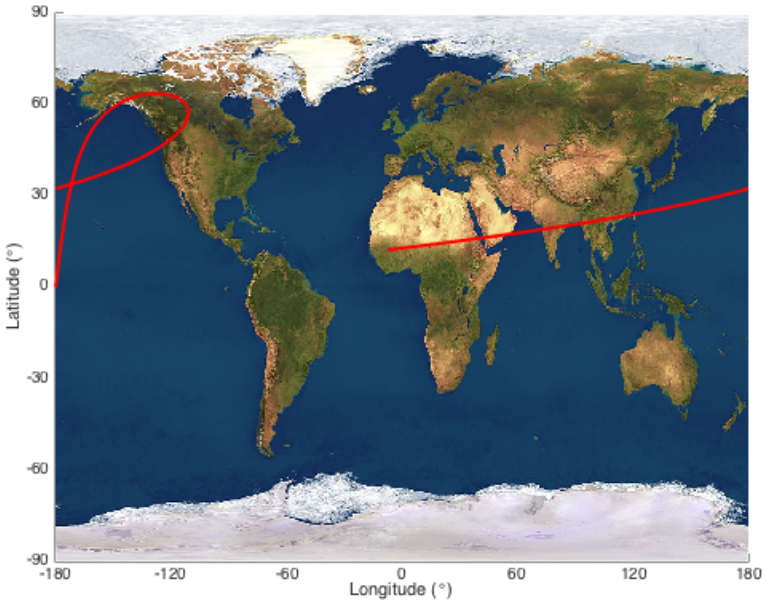

Figure 2.4: Ground Track after 1 day

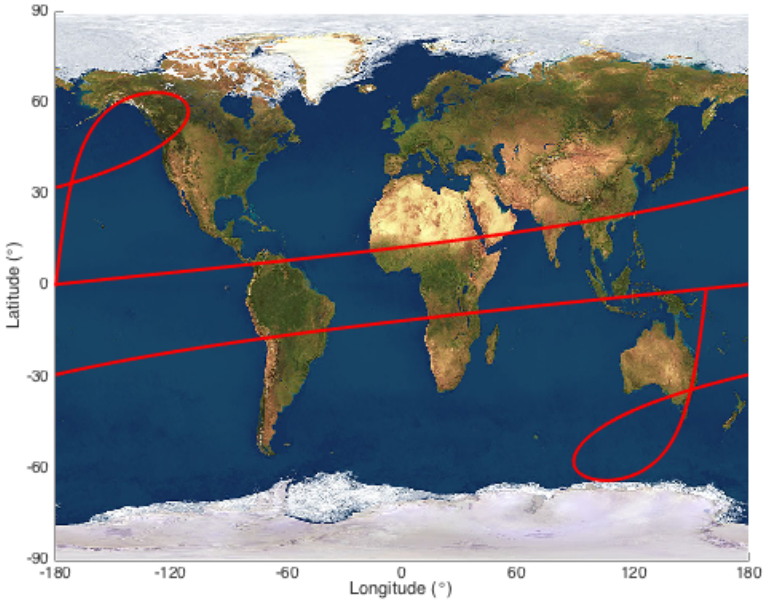

Figure 2.5: Ground Track after 1 period

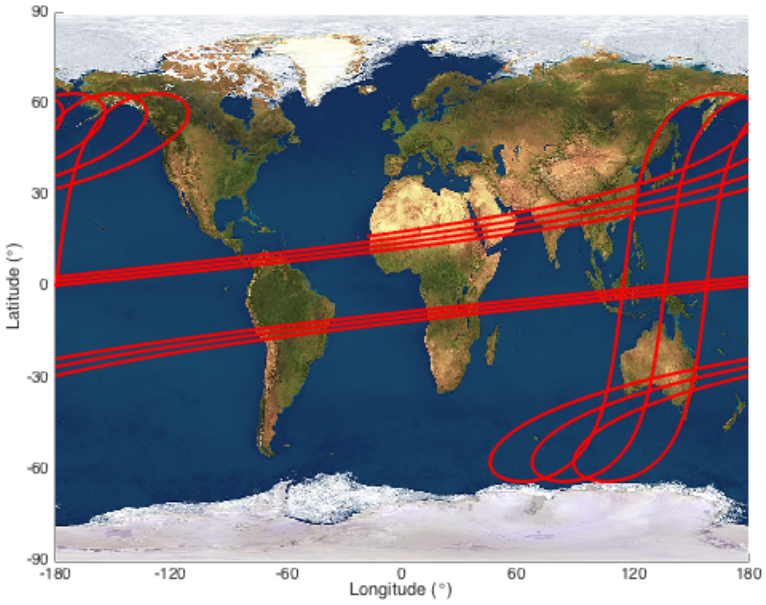

Figure 2.6: Ground Track after 10 days

2.1.3 Environment Description

The S/C operates on a Highly Elliptical Orbit around Earth, spending a big amount of time far from the Earth, operating in deep space conditions.
This last consideration will drive the choice of the orbit in which the S/C will operate its mission, since the disturbances which comes from orbital perturbation and radiations must be taken into account.
During its life-cycle, in fact, the S/C will be continuously exposed to the effects given by the Earth's oblateness (J2), the lunar gravitational field and solar radiation pressure which will lead to a variation of the orbit. If not properly corrected, these kind of perturbations could influence the performances of the mission, therefore the S/C must be able to properly correct its trajectory in order to limit the effects of those perturbations.
A source of disturbance for electronics comes from radiations, under the form of ionizing particles. Those kind of particles can have different origins: they could be trapped in Van Allen belts; they could come from solar wind or solar flares; they could be cosmic rays. Ionizing particles interact with the electronic parts of the payload, causing short-circuit, latch-up events and single event upset which would lead to the malfunction of the electronics itself. In the subsections below, a brief analysis of each orbital perturbation and radiation source has been performed.

Orbital Perturbations

- **Earth's Oblateness (J2)**
  This perturbation is given mainly by the fact that Earth is not a perfect sphere. The perturbing potential of Earth can be divided into two contributions: the zonal harmonic

potential and the tesseral harmonic potential; their effects on the operative orbit are the precession of perigee and the nodal regression. A MATLAB simulation that shows the effect of Earth's Oblateness on the orbit has been performed (fig. 2.7).

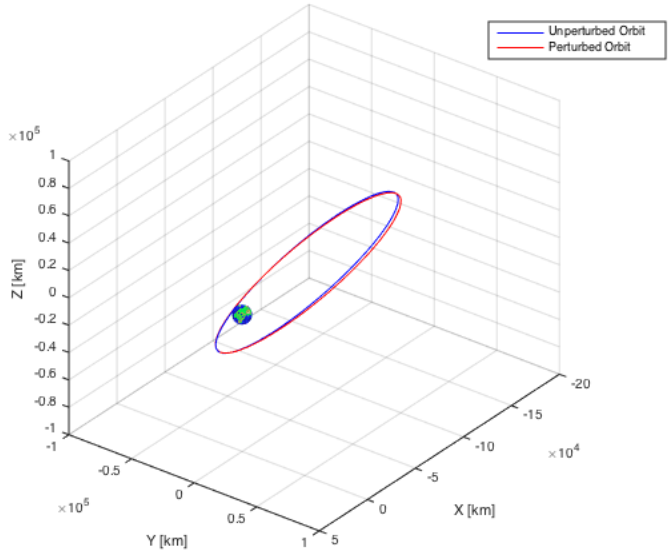

Figure 2.7: Perturbation due to J2 (over 1 year)

- **Lunar Gravitational Field**
  The lunar gravitational field has a perturbation effect on the orbit of the S/C. Its main effects are changes of inclination, eccentricity and ω. Due to the fact that Zwicky works on a HEO, this effects can be significant. A MATLAB simulation that shows the effect of lunar gravitational field on the orbit has been performed (fig. 2.8).

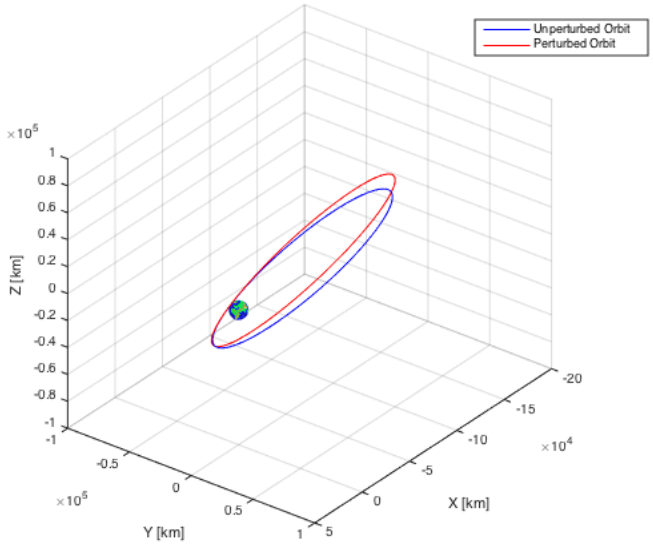

Figure 2.8: Perturbation due to lunar gravitational field (over 1 year)

- **Solar Radiation Pressure**
  This perturbation is given by the continuous radiation coming from Sun. It affects mostly small bodies because of their high area-mass ratio and its main consequence is to circularize the orbit by decreasing eccentricity; however this perturbation has secular effects and, during the life-cycle of the satellite, the orbit is not strongly perturbed. A MATLAB simulation that shows this effect on the orbit has been performed (fig. 2.9).

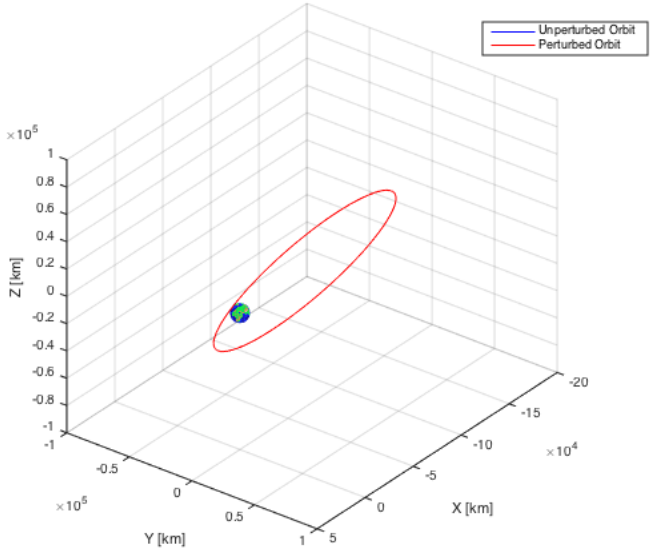

Figure 2.9: Perturbation due to SRP (over 1 year)

The total effects of the above mentioned perturbations on the orbit selected for Zwicky can be seen in fig. 2.10

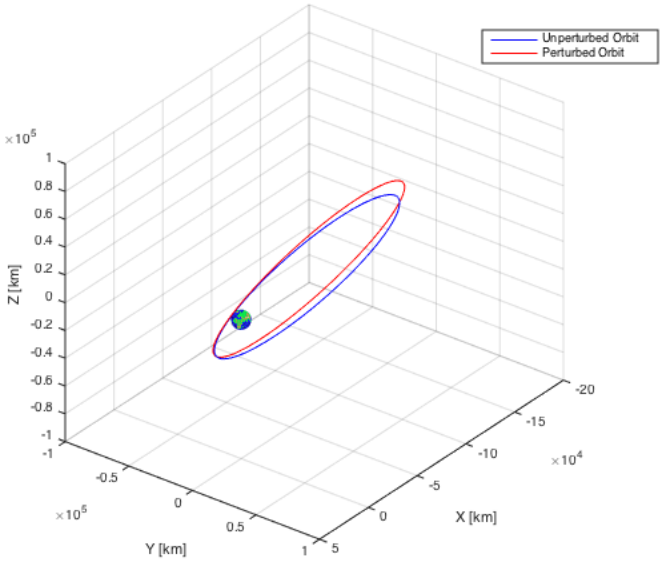

Figure 2.10: Perturbation due to J2, Moon and SRP (over 1 year)

Radiations

- **Trapped Protons and Electrons Flux**
  A lot of charged particles gets trapped into Van Allen belts. Below these radiation belts is possible to consider the environment almost safe.
  What happens however, is that inside of these belts a very high density of charged particles would hit the surface of the S/C. A SPENVIS simulation of the trapped proton flux and trapped electron flux has been performed for the selected orbit (fig. 2.11).

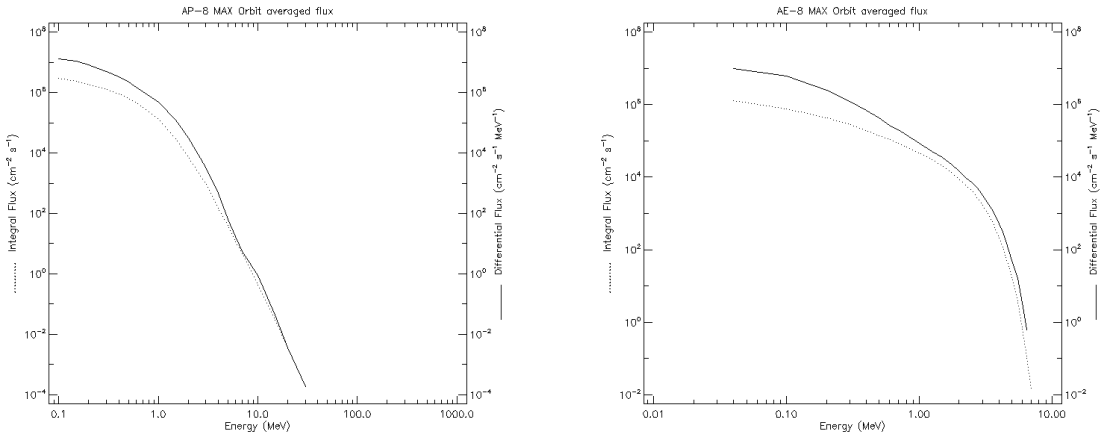

(a) Trapped Proton Flux

(b) Trapped Electron Flux

Figure 2.11: Trapped particles Flux

- **Solar Wind**
  The Solar Wind is a continuous neutral plasma that is directed approximately away from the Sun. Along the years it changes speed, density, magnetic field strength and direction. This plasma is composed of a relatively constant flux of charged particles, mainly electrons and protons, plus ions of various elements. A SPENVIS simulation of the effects of charged particles like Protons and Heavy Ions coming from the sun has been performed (fig. 2.12).

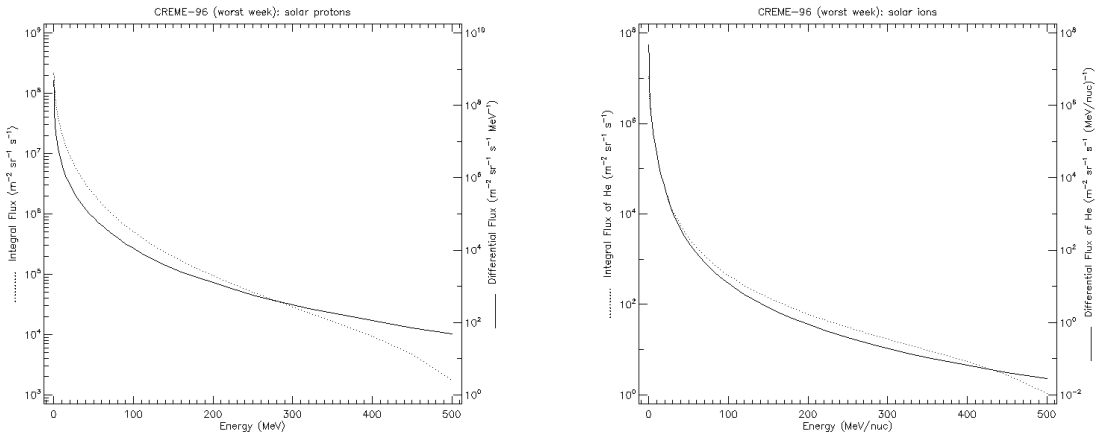

(a) Solar Proton Flux

(b) Solar Heavy Ion Flux

Figure 2.12: Solar particles Flux

- **Galactic Cosmic Rays**
  The Cosmic Rays are high-energy charged particles, originated and accelerated outside of the solar system, they are approximately made of 83% of protons, 13% alpha particles, 3% of electrons and 1% heavy ion nuclei. A SPENVIS simulation of ions' effects has been performed (fig. 2.13).

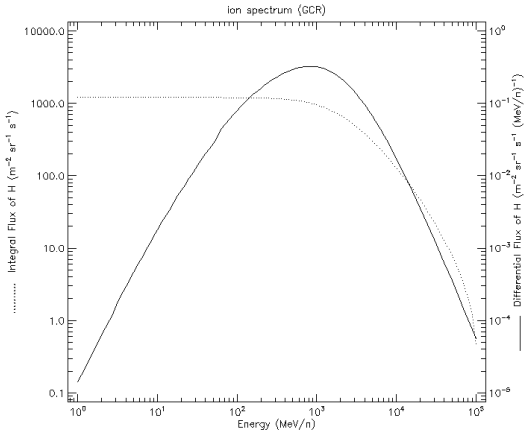

Figure 2.13: GCR Ion Spectra

- **Single Event Upset**
  A single event upset (SEU) is a change of state caused by one single ionizing particle (ions, electrons, photons...) striking a sensitive node in a micro-electronic device, such as in a microprocessor, semiconductor memory, or power transistors.
  The state change is a result of the free charge created by ionization in or close to an important node of a logic element (e.g. memory "bit"). A SPENVIS simulation of SEU's effects has been performed (fig. 2.14 and 2.15).

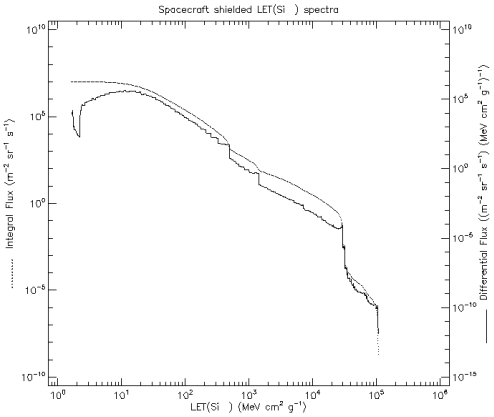

(a) Spacecraft shielded LET spectra

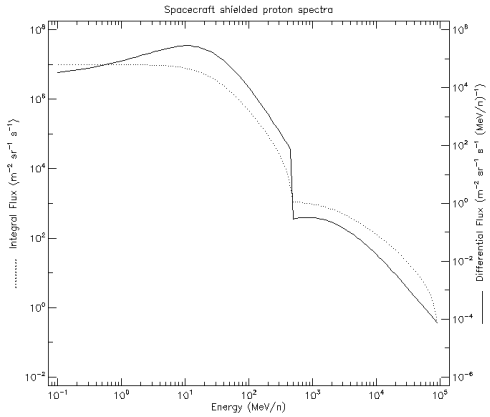

(b) Spacecraft shielded proton spectra.

Figure 2.14: Short-term SEU rates and LET spectra

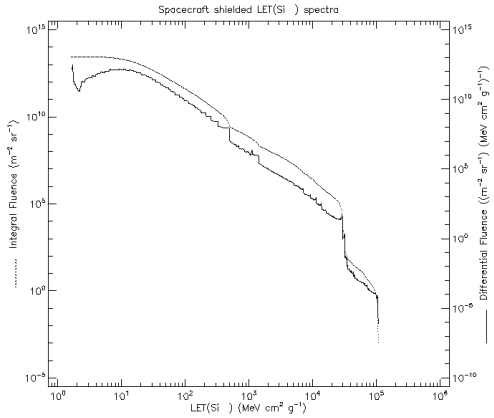

(a) Spacecraft shielded LET spectra

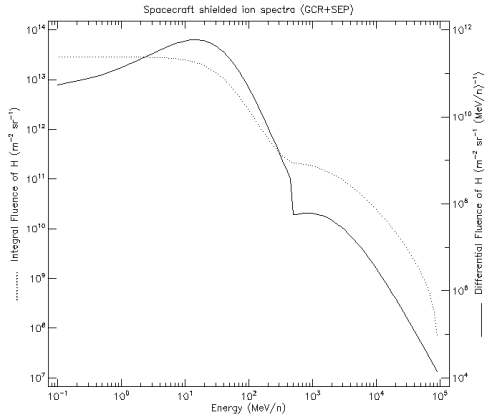

(b) Spacecraft shielded ion spectra

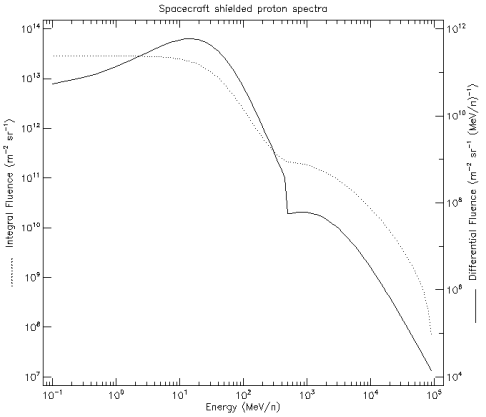

(c) Spacecraft shielded proton spectra

Figure 2.15: Long-term SEU rates and LET spectra

Total Ionizing Dose

The total ionizing dose predicted for an Al slab with SHIELDOSE-2 model, for a highly elliptical orbit mission of seven years, is shown in figure 2.16

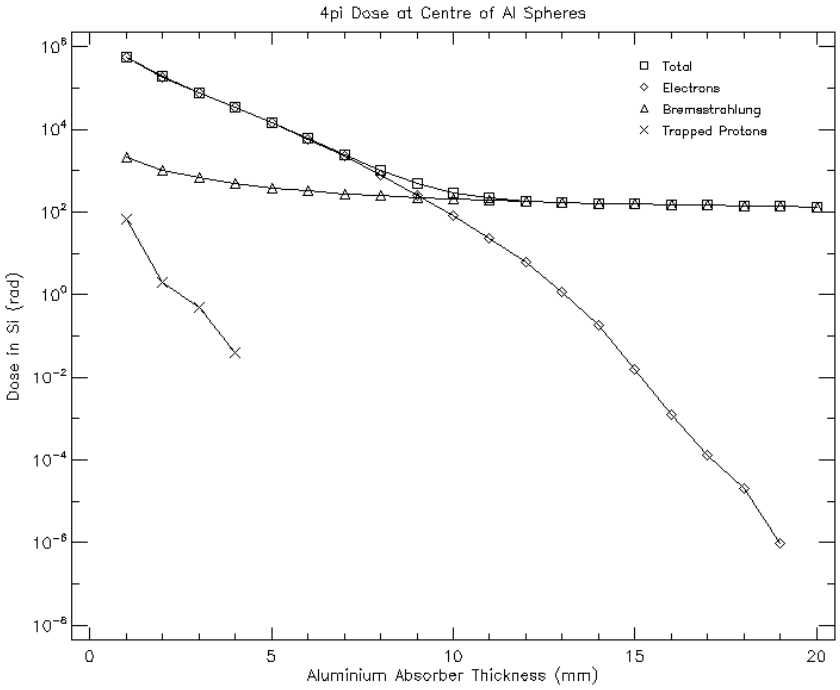

Figure 2.16: Total Ionizing Dose

2.2 Overview of the Concept

Here a brief description of the Technical Flowchart in Fig. 2.17 is provided. The science that Zwicky is required to perform consists in the analysis of the weak lensing and red shift phenomena. An optical telescope and two detectors are needed. The data collected by the detectors must be handled by the OBDH that has a CPU capable of doing on-board processing and a storage to save the information. Both the telescope and the detectors have an operating temperature range in which they must be kept, so a thermal subsystem must be present in order to control the temperature on the payload. The instruments of Zwicky must be kept running, so a power subsystem capable of controlling and distributing power is required.
Zwicky must be able to look to different region of the sky to meet the requirements defined in [21], so the S/C shall be able to perform slew maneuvers with an high degree of precision.
Last but not least, a structural subsystem capable of damping vibrations must be present.
All the subsystems shall be interfaced with the S/C.

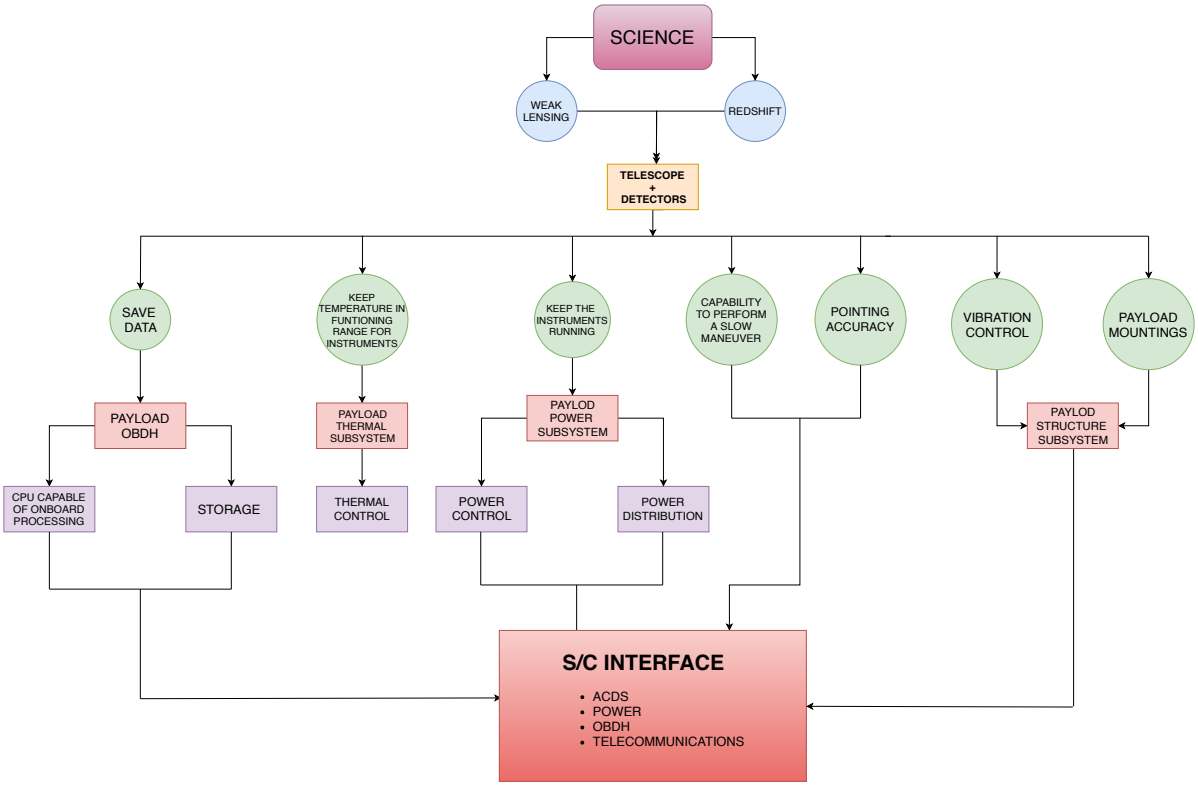

Figure 2.17: Technical Flowchart

2.2.1 Optical Architecture

Optical System Trade-Off

The aim of the mission is to collect data and images in visible and infrared spectrum of light; in order to do this the best solution is the usage of an optical telescope. There are mainly three kinds of telescope available:

- Refracting (using lenses to collect and focus light)
- Reflecting (using mirrors to collect and focus light)
- Catadioptric (using both mirrors and lenses)

Due to the necessity to look at the infrared spectrum, the use of lenses is not convenient, because those usually absorb the infrared spectrum, except for some particularly expensive and complex lenses design. As consequence, refracting and catadioptric options have been discarded and the reflecting type has been considered the optimal solution.
Reflecting telescopes are divided in different categories in function of the position of mirrors and eyepiece. The choice of the category is driven by the following statements:

1. the telescope operates in space, on a highly elliptical orbit; limitations in terms of weight and dimensions have to be considered due to launcher capability constraints.
2. the telescope has to look at very far deep space objects (DSO) with a sufficiently high detail.
3. the telescope has to avoid primary aberrations and other phenomena that could bring to low quality data acquisition.

As a consequence of these considerations the choice of the telescope falls on the **Cassegrain** category, which is also one of the simplest, sturdy and low cost architecture that can guarantee also high performances. In particular, two possible configurations have been identified to correct the aberrations phenomena: the three-mirrors configuration and the two-mirrors configuration.

The aberrations problem

Aberrations in an image are the result of an optical system failing to produce an exact point-to-point correspondence between the source and its image. There are four on-axis primary aberrations: spherical aberration, coma, astigmatism, field curvature.

- **Spherical aberration:** rays issuing from a source at infinite distance on axis do not converge all in the same point. The focus of the marginal rays is different from the focus of the par-axial rays. In two-mirror systems, spherical aberration is due to the fact that the mirrors do not have matching conic constants. This aberration is eliminated by using a paraboloid mirror.
- **Coma:** rays issuing from an off-axis source do not converge at the same point in the focal plane. This creates a blur which resembles a comet, hence the name. Coma aberration is field-dependent and increases linearly with the off axis angle. More present for fast optics, so small f-ratio number. In a Cassegrain telescope coma can also appear when

the secondary mirror axis is not exactly coaxial with the primary mirror axis. A correct on-axis positioning of the secondary mirror can eliminate this type of aberration.

- **Astigmatism:** the focus of rays in the plane containing the axis of the system and an off-axis source is different from the focus of rays in the perpendicular plane. In order to correct astigmatism, dedicated lenses or a tertiary mirror with a particular design are needed.
- **Field curvature:** image does not form on a "plane," but on a curved surface. In case of astigmatism absence, the image would be formed on a curved surface called the Petzval surface. In order to correct this aberration, a tertiary mirror or a dedicated design of the secondary mirror are needed.

The need of avoiding aberrations comes from the necessity to obtain high quality images in the visible spectrum without any distortion of light due to the instruments. The presence of primary aberrations could bring to large errors in the data related to the detection of distorted light coming from gravitational lensing phenomena, making all measurements useless. Astigmatism is the most problematic aberration due to the fact that its correction is not simple, in particular at high order. A low order aberrations correction could not be enough to obtain clear acquisition data in order to perform gravitational lensing studies with high quality. A tertiary mirror is able to correct at the third order this aberration, ensuring a sufficient accuracy of the data; this explains the choice of the three-mirrors configuration as baseline solution.

Cassegrain: three-mirrors architecture (Baseline solution)

Known as three-mirror anastigmatic or Korsch configuration, it is one of the most modern solutions adopted for space telescopes due to its high quality correction of typical main telescopes aberrations. It is characterized by relative compact size and the design that has been adopted consists in the following elements:

- Primary mirror
- Secondary mirror
- Tertiary mirror
- Two plane reflecting mirrors
- Dichroic filter
- Moving mirror

Primary and secondary mirrors are able to correct spherical aberrations and coma, while the tertiary mirror is able to correct the astigmatism and the field curvature.
The light is collected through the aperture of the telescope and is focused by the primary mirror on the secondary. Then the light enters inside the internal part of the telescope where a first reflecting mirror sends it on the tertiary mirror. This mirror is characterized by a particular curvature that enables the correction of the astigmatism and sends the light to the detectors through a second reflecting mirror.

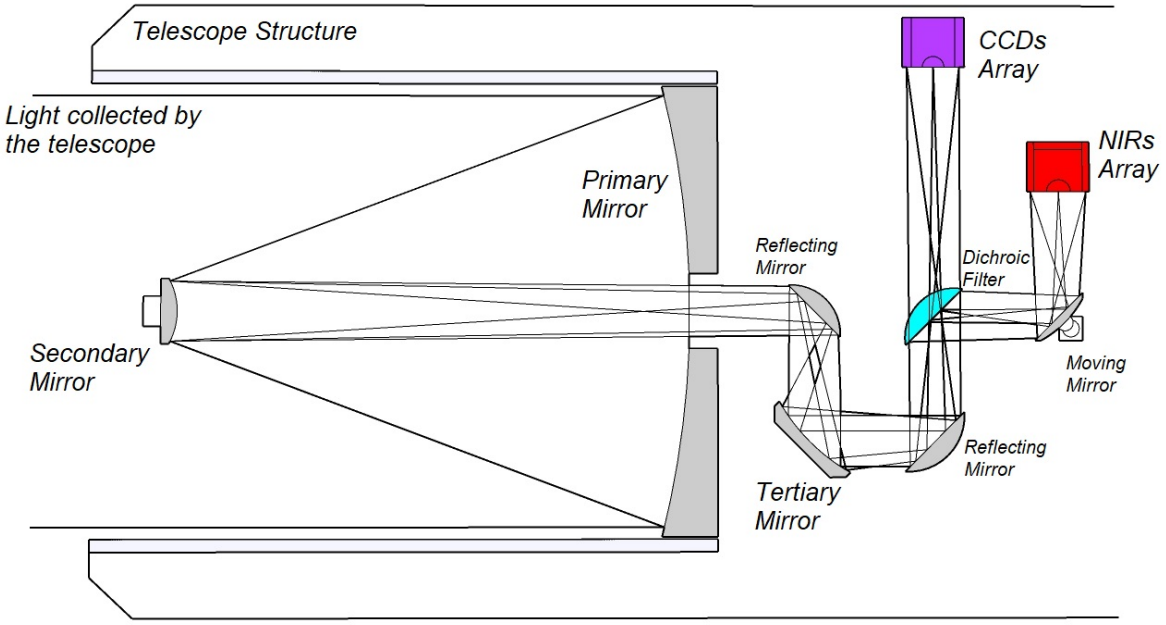

Figure 2.18: Three-mirror configuration scheme

Before the light reaches the detectors, other two elements are positioned in between.
The first element is a dichroic filter, a particular lens that allows the passage of the visible light while reflects the infrared radiation; in order to work properly it has to be inclined of 45° with respect to the incoming light beam direction.
The second element is a moving mirror positioned between the spectrometer and the dichroic. This is an essential component for the proper operation of the baseline spectrometer, in fact it allows the selection of the line of light that has to be focused on spectrometer's imaging sensors.

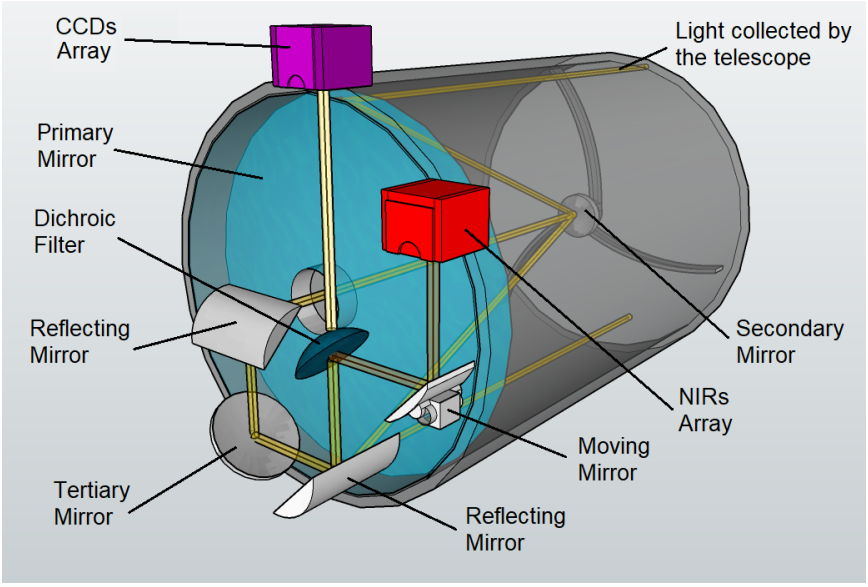

Figure 2.19: Three-mirror configuration 3D scheme

Cassegrain: two-mirrors architecture (Back-up solution)

The alternative solution chosen as back-up of the baseline previously defined is the two-mirrors configuration, also called Ritchey-Chretien. In this solution, as in three-mirrors case, a dichroic lens is added in order to filter the visible light directly to the related detectors (CCDs) and reflects the infrared light to a fixed mirror, finally sending the light to the spectrometers. The use of a different spectrometer, as will be shown in the section 2.2.5, allows to remove the moving mirror used in the baseline.
The two-mirrors architecture is capable of correcting spherical aberration, coma and, with a particular design of the secondary mirror, can correct also the field curvature. However it is not possible to correct the angular astigmatism. In order to correct the astigmatism a specific lens at the entrance of the detectors is needed, as in Hubble space telescope's architecture, but in any case it is not possible to reach the same level of correction of the three mirrors solution. With this configuration the performance is lower in terms of accuracy of image resolution; in particular for the gravitational lensing lower quality data is expected. However the two mirror configuration is simpler, sturdier and has already flew in space for over thirty years.

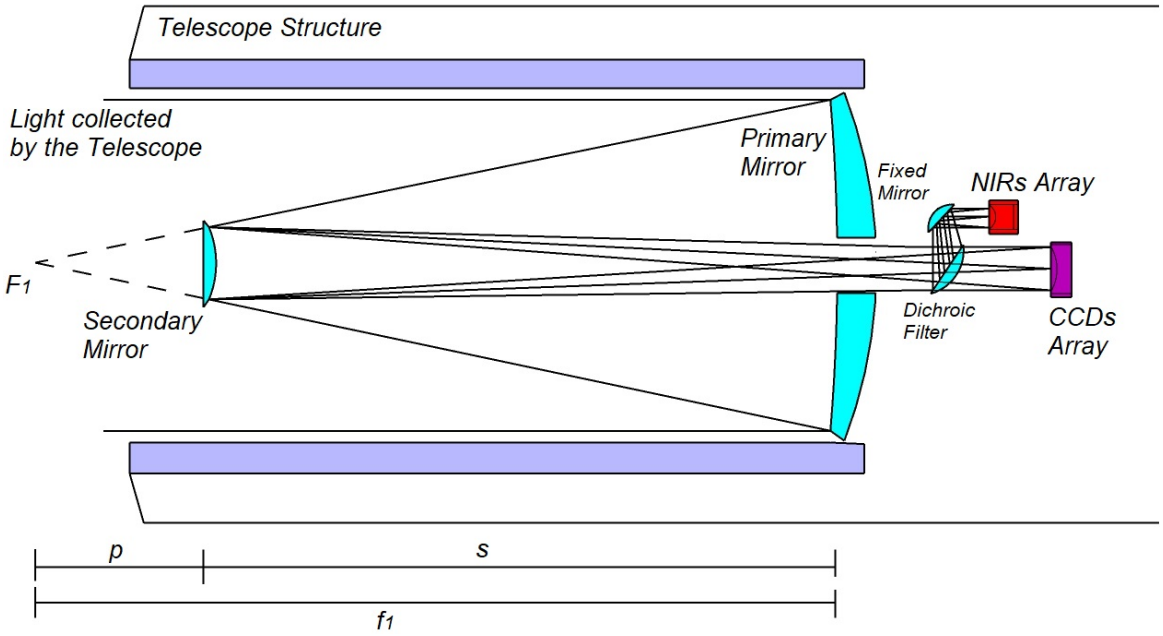

Figure 2.20: Two-mirrors configuration scheme

2.2.2 Optical Design Process

Definition of the Field of View

The starting point for the design of a space telescope is the selection of the field of view. The field of view is something inversely proportional to the resolving power of the telescope. It is possible to start the definition of the field of view identifying the dimensions of the object of interest: far galaxies and galaxy clusters.
In order to have a reference of the average characteristic size of galaxy clusters, the Abell galaxy clusters catalogue has been considered. The clusters have different dimensions, from some minute to few degrees, with a density of galaxy that can go from 3 up to 80 galaxies per square-degrees. Considering that the average galaxy clusters size inside the Abell catalogue is in the order of 30 arcmin, this dimension is taken as reference, selecting as consequence a **Field of view** of:

$$FOV = 0.50\,\mathrm{deg}^2$$

Resolution, Focal Length and Aperture diameter of the telescope

The resolution of a sensor is the smallest difference between two measurement units; spatial resolution is the smallest angular or linear separation between two objects resolvable by the sensor.
Typically, the spatial resolution should be less than half of the size of the smallest object of interest.
So, if the telescope needs to see clearly a single galaxy inside the cluster (the smallest galaxy can be considered around few seconds of angular diameter), it needs to have a spatial resolution in the order of fraction of arc-second. (Typical resolution 0.1 arcsec for a single telescope; 0.001 arcsec for an array of interferometers)
Using a single telescope means that the optical sensor needed for deep space object observation, like galaxy clusters, has to guarantee at least the highest typical value of reachable resolution, so the typical limiting value of 0.1 arcsec has been considered.
The computation of the focal length is performed after the selection of the detectors, to understand if the selected field of view and resolution are acceptable.
In order to compute the focal length a detector for the visible light has been selected. Basing on the available imaging sensors already on the market, different simulations with different types and number of CCD detectors has been performed considering the following formula:

$$\frac{rd}{f} = \frac{sin(\theta_{FOV})}{cos(\theta_{FOV})} = tan(\theta_{FOV})$$

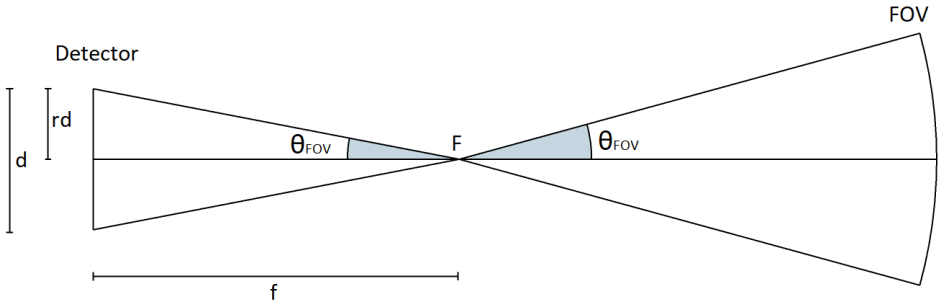

The CCDs have been set as main detectors for the definition of telescope resolution due to the interest on a higher resolving power in visible respect in the infrared.This because to perform a good quality data acquisition for the gravitational lensing a high resolution in the visible is needed, and for the same restriction the CCDs have to operate at least at minimum working resolution.
Trying different CCDs it has been obtained that with a field of view of $0.50\,\mathrm{deg}^2$ it is not possible to maintain an angular resolution of 0.1 arcsec for the telescope, because the selected detectors would not guarantee the minimum working condition.
A CCD with a sufficiently high resolution has been chosen from the available ones, maintaining the same FOV as before; the resolution of the selected CCD is equal to 0.155 22 arcsec.
Knowing the resolution of the CCD is possible to define the minimum working condition, obtaining the telescope resolving power with the following equations:

$$\text{Telescope resolution} = \text{Min resolution} = \frac{CCD_{resolution}}{2} = \frac{0.15522}{2} = 0.077\,61\,\text{arcsec}$$

The focal length obtained for telescope using the chosen detector is:

$$f = 19.9328\,\text{m}$$

An array of 4x4 CCDs of 61.5 mm of diameter, with a number of 4100×4100 pixels for each CCD and a dimension of 15 µm for each single pixel, has been selected.
Knowing the desired resolution, it is possible to compute the diameter aperture of the telescope, considering the diffraction limit wavelength parameter. Usually telescopes work very close to this value, so, as consequence, the Rayleigh equation has been chosen to design the circular aperture:

$$\theta = 1.22 \times \frac{\lambda}{D}$$

where λ is the wavelength, θ is the angular resolution and D is the diameter of the aperture.
θ and λ are known, so it is possible to compute D from the up-written formula.
Considering the chosen wavelengths, from 400 nm up to 1800 nm, and knowing the resolution, 0.077 61 arcsec, the obtained results are listed in Table 2.2.

λ[nm]	D[m]	λ[nm]	D[m]	λ[nm]	D[m]	λ[nm]	D[m]	λ[nm]	D[m]	λ[nm]	D[m]
400	1.296	650	2.107	900	2.918	1150	3.728	1400	4.539	1650	5.349
450	1.459	700	2.269	950	3.080	1200	3.890	1450	4.701	1700	5.512
500	1.621	750	2.431	1000	3.242	1250	4.053	1500	4.863	1750	5.674
550	1.793	800	2.593	1050	3.404	1300	4.215	1550	5.025	1800	5.836
600	1.945	850	2.756	1100	3.566	1350	4.377	1600	5.187		

Table 2.2: Diameter dimension for different wavelengths

As shown in Table 2.2, for each wavelength, maintaining the same resolution, very different results for the aperture have been found. It is not possible to create a telescope with a variable aperture that goes from 1 up to 5 meters, so a single fixed value for the diameter has been chosen and as consequence a loss of resolution in certain wavelengths.
In order to acquire the gravitational lensing phenomenon data, a particularly good resolution in the visible spectrum is needed to perform a good separation of close objects, more than in the infrared one. It is reasonable to assume that the main wavelength in which the resolution of 0.077 61 arcsec is required is in the middle of the visible spectrum, 500 nm to 600 nm.
After this consideration, a diameter of 1.80 m has been chosen and a new computation has been performed to evaluate the resolutions for each wavelengths; the results are shown in Table 2.3.

λ[nm]	θ[as]	λ[nm]	θ[as]	λ[nm]	θ[as]	λ[nm]	θ[as]	λ[nm]	θ[as]	λ[nm]	θ[as]
400	0.0559	650	0.090	900	0.125	1150	0.160	1400	0.195	1650	0.230
450	0.063	700	0.097	950	0.132	1200	0.167	1450	0.202	1700	0.237
500	0.069	750	0.104	1000	0.139	1250	0.174	1500	0.209	1750	0.244
550	0.076	800	0.112	1050	0.146	1300	0.181	1550	0.216	1800	0.251
600	0.083	850	0.118	1100	0.153	1350	0.188	1600	0.223		

Table 2.3: Resolution for each wavelength [as = arcsec]

As shown in the table, with an aperture of 1.80 m it is possible to obtain a resolution of around 0.076 arcsec for the visible light and a resolution around 0.2 arcsec for the near-infrared.

Mirrors sizing

Knowing all the data reported in the previous part, in addition to the primary mirror f-ratio $N_1 = f/15$ and the normalized backfocal distance $\beta = 0.35$, a sizing of all the others mirrors inside the telescope has been performed. Focusing on the main mirrors the following formulas have been considered:

N_i: f-ratio of the mirror i
f_i: focal length of the mirror i
m: magnification
D_i: diameter of the mirror i
Ob_{ratio}: obscuration ratio
s: distance between primary and secondary mirror
b: backfocal distance
β: normalized back focal distance
c_{mi}: half of the light beam width that a mirror i have to cover
d_{mi}: distance between two mirrors
r_{mi}: radius of the mirror i
k_i: conic constant of the mirror i

[1]	$f_1 = D_1/N_1$	Primary mirror focal length
[2]	$f_2 = s + b$	Secondary mirror focal length
[3]	$m = f/f_1$	Magnification of the secondary mirror
[4]	$D_2 = D_1 \times \frac{f_1+b}{f+f_1}$	Secondary Mirror Diameter
[5]	$b = \beta \times f_1$	Backfocal distance
[6]	$O_{ratio} = D_2/D_1$	Obscuration ratio
[7]	$s = \frac{f-b}{m+1}$	Primary secondary separation
[8]	$N = f/D_1$	Total f-ratio
[9]	$d_{3m} = \%distance \times b$	Distance of the tertiary mirror respect to the focus
[10]	$r_3 = \frac{c_{3m}}{cos(inclination_{3m})}$	Radius of the tertiary mirror (approximate)
[11]	$k_1 = -1 - 2 \times \frac{1+\beta}{m^2 \times (m-\beta)}$	Primary mirror conic constant
[12]	$k_2 = -(\frac{m+1}{m-1})^2 - \frac{2 \times m \times (m+1)}{(m-\beta)/(m-1)^3}$	Secondary mirror conic constant

Table 2.4: Properties of the main mirrors

The distance between the different reflecting mirrors is chosen in order to obtain the correct focus of the light on the detectors. The tertiary mirror has to be designed under some considerations. It shall have a focal length of 2.0 m, a diameter and inclination to collect the light coming from the first reflecting mirror and to redirect it with a changed inclination of 90° and a particular curved surface to correct astigmatism and field curvature aberrations.
Table 2.5 shows the dimension, the focal length and the conic constant data obtained for the main mirrors. A preliminary approximation of the needed diameter of the tertiary mirror is also considered with an assumed ideal inclination of 45°; in a similar way also data for the Dichroic filter and the moving mirror have been reported.

	Diameter [m]	Focal Length [m]	Conic Constant
Primary Mirror	1.80	2.3919	-1.0048
Secondary Mirror	0.26	2.8831	-7.689e+03
Tertiary Mirror	0.37	2.0	-
Dichroic Filter	0.30	-	-
Moving Mirror	0.27	-	-

Table 2.5: Mirrors data

Regarding the obscuration ratio, this value represents how much area of the primary mirror is obscured by the secondary mirror with a consequentially loss of the light collected. An obscuration ratio lower than 0.15 is optimal as the primary mirror is not obscured by the secondary mirror, with no losses on the collection area. The obscuration ratio of Zwicky telescope is 0.144.
The other mirrors inside the system are only reflecting mirrors. These mirrors are supposed to be flat and with an inclination respect to the horizontal direction that must be enough to allow the passage of the light without obstruction, in order to direct it to the detectors or to the other mirrors. The inclinations considered for the mirrors are shown in Table 2.6.

	Reflecting mirror 1	Reflecting mirror 2
i	45°	45°

Table 2.6: Mirrors inclination

For the reflecting mirrors the equations used to obtain the diameter, the distance between the mirrors and the distance between the detector and the relative mirror (Dichroic for the CCDs and moving mirror for the Spectrometers) are shown in Table 2.7.

[13]	$d_{mirror} = \%distance \times b$	Distance of the mirror respect to the focus before the tertiary mirror
[14]	$d_{mirror} = \%distance \times f_3$	Distance of the mirror respect to the focus after the tertiary mirror
[15]	$r_{mirror} = \frac{c_{mirror}}{cos(i_{mirror})}$	Radius of the mirror
[16]	$D_{mirror} = 2 \times r_{mirror}$	Diameter of the mirror
[17]	$CCD_{distance} = f_3 - d_{dichroic}$	CCDs distance from the Dichroric
[18]	$NIRs_{distance} = f_3 - d_{movingmirror}$	NIRS distance from the Moving Mirror

Table 2.7: Mirrors position equations

The results of these equations are shown in Table 2.8. An observation on the diameters has to be done. The values obtained are the minimum needed to allow the reflection of the light beam; this means that the mirrors' diameters are not the real ones, but have to be oversized to guarantee an area wide enough for a correct reflection. A 5% over-size is consider for the real dimension.

Reflecting mirrors	Diameter [m]	Diameter oversized [m]	H separation [m]	V separation [m]
Mirror 1	0.294	0.310	0.502 from Primary	0.0
Tertiary	Previus results table	-	0.0 from the Mirror 1	0.502 from the Mirror 1
Mirror 2	0.337	0.354	0.50 from the Tertiary	0.0 from the Tertiary
Dichroic	0.303	0.318	0.0 from the Mirror 2	0.50 from the Mirror 2
Moving Mirror	0.273	0.287	0.50 from the Dichroic	0.0 from the Dichroic

CCD distance from the Dichroic [m]	1.0
NIRs distance from Moving Mirror [m]	0.50

Table 2.8: Detectors distances

In the end, knowing the inclinations, positions and dimensions of all the mirrors and detectors inside the telescope, a preliminary estimation of the dimension of all the system is performed, obtaining that the telescope has to be approximately 2.5 m long and 2.5 m large.

Materials selection for the mirrors

Mirrors used in space application have different and very strictly requirements in order to guarantee the correct reflection of the light:

- they need to be dimensionally stable over time for the optical figure to be retained for decades;
- they need to have low internal stress not to deform when material is removed during the figuring process or over time due to stress relaxation;
- they do not have to deform when subjected to environmental temperature gradients;
- they need to have sufficient mechanical rigidity and strength to allow both handling and mounting;
- they need to have a fine polish surface and to be coatable by vacuum-deposition methods;
- in the case of cryogenic applications, they must not undergo structural changes when cooled to very low temperatures;

As consequence of these limitations, the identified main typical materials adopted in space telescope mirrors are:

1. **Borosilicate:** low-expansion borosilicate glasses offers the possibility of lightweighting by direct honeycomb casting and the added advantage of lower cost. Usually not used after the 1960s due to development of ultralow-expansion ceramic or fused silica, which have the same favorable polishing properties but coefficients of thermal expansion 100 times lower.
2. **ULE fused silica**: it is fused silica doped with titanium, which results in an expansion coefficient at room temperature that is 20 times lower than that of pure fuse silica. It is

produced in "boules" of about 1.2 meters in diameter. Lower stiffness respect to Borosilicate maintaining the same density.

3. **Low-thermal-expansion glass ceramics**: devitrified glasses are two-phase materials in which the balance between the crystalline phase and the amorphous phase can be set to minimize the overall thermal expansion coefficient in a given temperature range. Higher density but lower stiffness respect to borosilicates. Glass ceramic is difficult to cast in complex shapes such as honeycombs.

4. **Silicon Carbide**: known under the trade name Carborundum, is one of the hardest synthetic materials. It has excellent thermal diffusivity and its high specific stiffness makes it one of the ideal blank mirror material with attractive physical and mechanical performance.

5. **Beryllium**: one the lightest and stiffest metals, has an expansion coefficient higher than that of vitreous mirror materials, but high specific stiffness and thermal diffusivity. This makes it an outstanding choice for mirrors when very low areal densities are desired, as for space applications. Main drawback is the low reflectance in the visible spectrum around the 50% while is higher than the 98% for the infrared.

6. **Aluminum**: the main advantages of aluminum are low cost and high thermal conductivity. But aluminum's high coefficient of thermal expansion requires either temperature control in the case of space applications. This makes aluminum difficult to use for cryogenic applications because the differences in coefficient of expansion between nickel and aluminum lead to large deformations during cooldown.

Knowing these informations, in the Table 2.9 are shown the materials that have been identified as possible solution for the mirrors system.

Focusing Mirrors	Material	Reflecting Mirrors	Material
Primary	Silicon Carbide (SiC)	1	Silicon Carbide (SiC)
Secondary	Silicon Carbide (SiC)	2	Silicon Carbide (SiC)
Tertiary	Silicon Carbide (SiC)	Moving Mirror	Beryllium

Table 2.9: Material selected for the mirrors

Silicon carbide is the best solution due to the low thermal expansion and high stiffness property. Also very important is the reflectance of the material that is over the 98% for the visible light and up to the 90% for the infrared light. Beryllium, instead, is a good choice for the moving mirror because the light incoming is only in the Infrared spectrum and beryllium has a reflectance up to 95% in that spectrum.

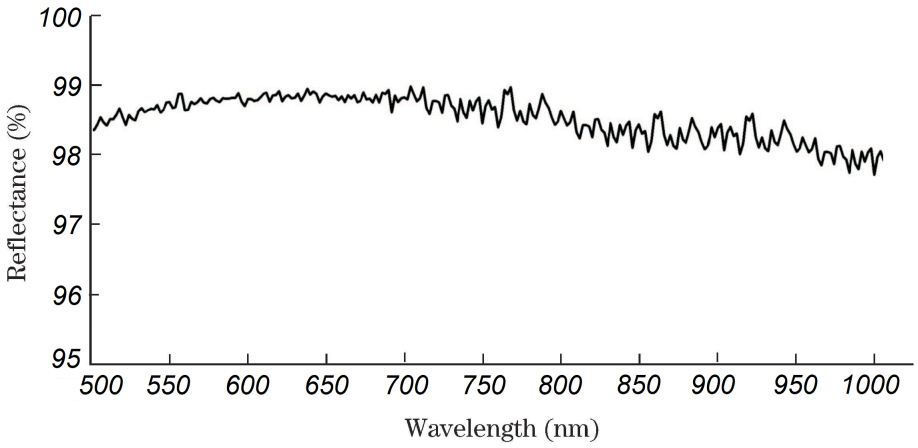

Figure 2.21: SiC reflectance in function of wavelengths

2.2.3 Dichroic filter

A selection of a dichroic filter has been made to split the beam of light in visible light and infrared radiation. Its function is to let selected a radiation range pass, reflecting the others. Two kind of filters can be distinguished:

- **Short Wave Pass (SWP)**: The pass band is to the left of the transition slope, the longer wave length is reflected.
- **Long Wave Pass (LWP)**: The pass band is to the right of the transition slope, the shorter wave length is reflected.

(a) LWP example

(b) SWP example

Figure 2.22: Radiation filters

Telescope's architecture needs a reflection of the infrared radiation, so a SWP filter is selected. This kind of filters works usually for inclination of 45° with respect to the incoming light beam; the diameters that they can reach is of the order of 2 m and, using different materials with different refraction index, can be customized for the needed frequency. The coating materials used for a SWP dichroic filter are Silicon, Sapphire, Germanium and IR Quartz. The agency **KO (Knight Optics)** has been selected for the construction of the customized dichroic filter with the needed cut-off frequency of 0.9 µm.

Secondary mirror support structure selection

Different structures can be adopted to maintain in position the secondary mirror inside the telescope's tube. Each type of structure affects light propagation with different behaviour and, as consequence, with different diffraction phenomena. An analysis on diffraction pattern for possible structure has been performed with MATLAB, bringing the following results:

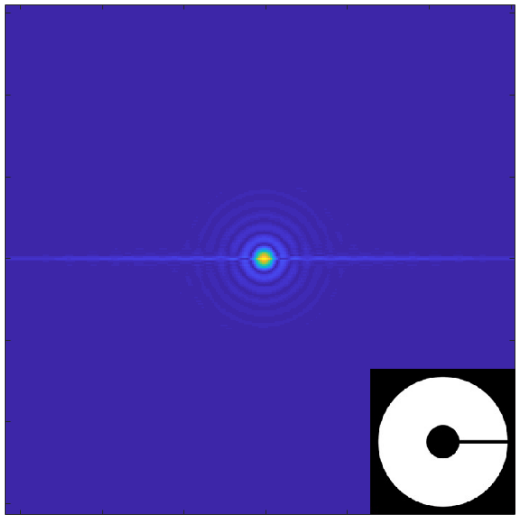

(a) 2 or 1 beams diffraction pattern

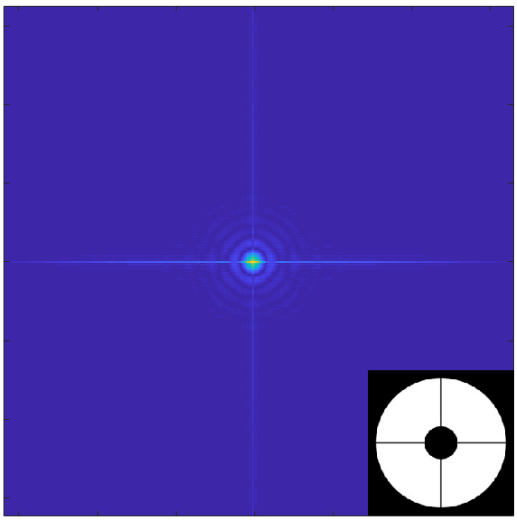

(b) 4 beams diffraction pattern

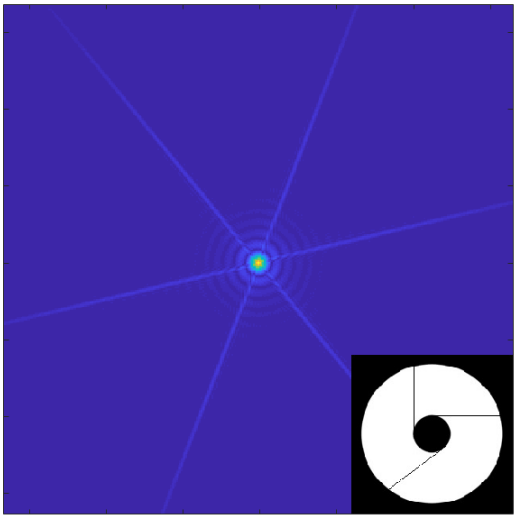

(c) 3 beams diffraction pattern

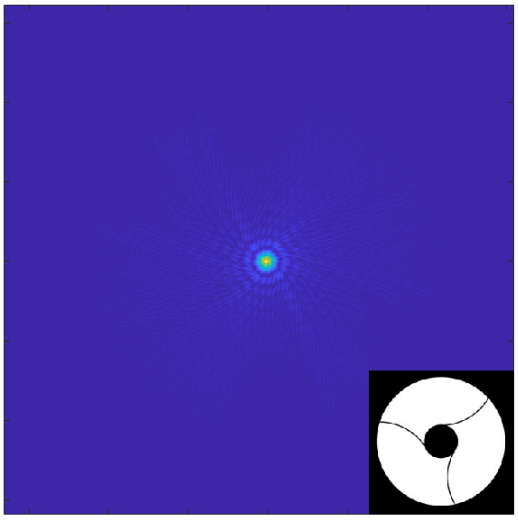

(d) 3 curved-beams diffraction pattern

Figure 2.23: Beam diffraction patterns

From the upper images it is possible to notice that a three curved-beams support structure considerably reduces the effects of the diffraction, respect to any kind of other structure,

increasing the images quality. As consequence, this particular configuration has been selected for the secondary mirror support structure of the Zwicky Space Telescope.

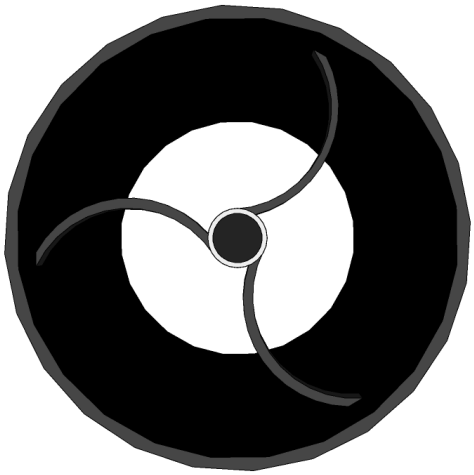

(a) Support structure frontal view art

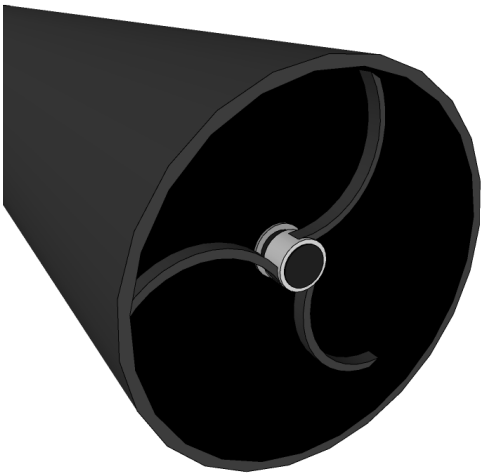

(b) Support structure 3D view art

Telescope internal tube coating selection

A coating on the inside of telescope's tube is needed, in order to absorb the incident light coming from different sources respect to the interested one and to prevent his reflection on the primary mirror.
A very smart choice for this purpose is the use of the Vantablack, the darkest material actually developed, 17 times darker than the paint used for the Hubble Space Telescope. The **Vantablack S-VIS** is available in spray paint form and is characterized by very high absorbance and low reflectance. Its characteristics are shown in Table 2.10.

Performance Data	
Total Hemispherical Reflectance %	VIS 0.3 % at 550 nm and 0.2 % at 700 nm
Total Hemispherical Reflectance %	NIR 0.2 % at 1400 nm
Coating thickness (average)	Typical 40μm Locally up to 100μm
Operating temperature range in vacuum or inert atmosphere	77 K to 973 K
Shock resistance	MIL STD 810 G Method 516.6
Vibration resistance	MIL STD 810 G Method 514.6
Mass / substrate area	0.7 mg/cm^2

Table 2.10: Vantablack S-VIS characteristics

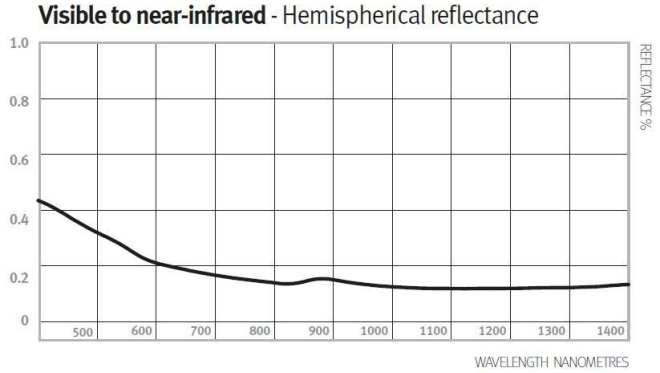

Figure 2.24: Vantablack S-VIS reflectance

2.2.4 Visible Detector: CCD

Visible detector trade-off

The detectors that have been considered as possible solution for the visible imaging are two: CCD (Charged Coupled Device) and CMOS (complementary metal-oxide semiconductor). The two sensors start at the same point, they have to convert light into electrons. A simplified way to explain how this procedure work, is to think of it as having a 2-D array of thousands or millions of tiny cells, each one transforming the light from one small portion of the image into electrons. After the collection of the electric charge the next phase is to read this value of accumulated charge for each cell in the image.
In a CCD device, the charge is actually transported across the chip and read at one corner of the array. An analog-to-digital converter turns each pixel value into a digital value. CCDs use a special manufacturing process to create the ability to transport charge across the chip without distortion. This process leads to very high-quality sensors in terms of fidelity and light sensitivity.
In most CMOS devices, there are several transistors at each pixel that amplify and move the charge using more wires. CMOS chips, on the other hand, use traditional manufacturing processes to create the chip, similar to the process used in manufacturing microprocessor. As each pixel on a CMOS sensor has several transistors located next to it, the light sensitivity of a CMOS chip tends to be lower. Many of the photons hitting the chip hit the transistors instead of the photo-diode. The main difference between the two types of sensor is shown in the Table 2.11.

Detector	
CCD	CMOS
high-quality images	good-quality images
low-noise images	more susceptible to noise
high sensitivity	low sensitivity
high-power sensor	low-power sensor
expensive manufacturing cost	cheaper manufacturing cost
mature technology	relative new technology
more number of pixels	lower number of pixels respect CCD

Table 2.11: CCD and CMOS comparison

Based on these differences, CCDs tend to be characterize by high-quality images with lots of pixels and excellent light sensitivity. CMOS sensors, have lower quality, lower resolution and lower sensitivity. So a CCD detector appears to be the best solution in order to perform the image acquisition at the required level both for the baseline and backup solution.

CCD Architecture

The CCD selected is already available on the market and is a CCD for astronomical and scientific imaging applications. It has been designed to provide a large image area and with a back-illuminated spectral response combined with very low read-out noise give exceptional sensitivity. The sensor has an image area having 4100×4100 pixels, split read-out registers at both top and bottom with charge detection amplifiers at both ends. The pixel size is 15 µm square. The image area has four separately connected sections to allow full-frame, frame-transfer, split full-frame or split frame-transfer modes. Depending on the mode, the read-out can be through 1, 2 or 4 of the output circuits. A gate-controlled drain adjacent to each of the registers is also provided to allow fast dumping of unwanted data. The output amplifier is designed to give very low noise at read-out rates of up to 3 MHz. The low output impedance simplifies the interface with external electronics and the optional dummy outputs are provided to facilitate rejection of common parasitic feed-through.

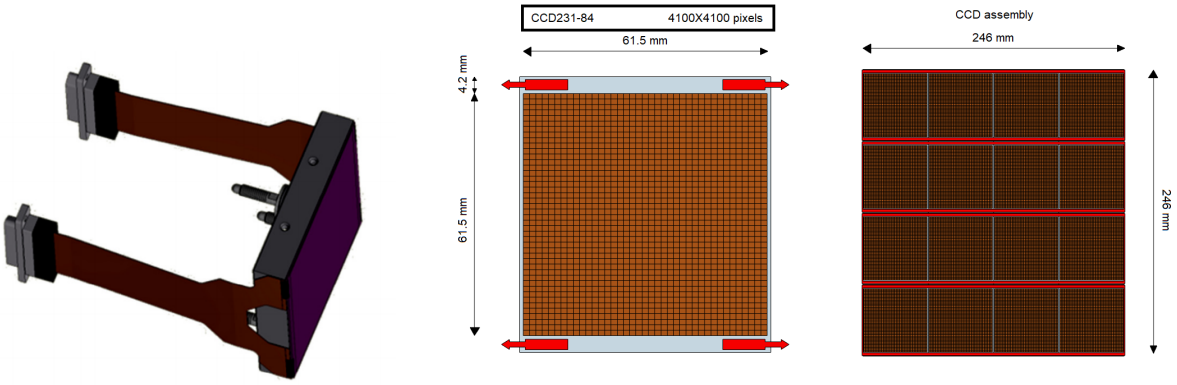

Figure 2.25: Single CCD and CCD array

CCD Type	Producer
CCD231-84 Back-illuminated Scientific Sensor 4100×4100 pixels	Teledyne e2V

Table 2.12: CCD information

The device can be supplied in two package types, both designed for cryogenic use, Silicon Carbide/flex-cable or Aluminum Nitride/PGA package. The Silicon Carbide/flex-cable package is chosen due to the possibility to allow close butting if needed. Specifications are tested and guaranteed by the producer at 173 K.
The number of CCDs needed for the telescope are a grid of (4×4) CCDs, and the total numbers of pixels of the array is 268.96 MP.
The main task of the CCDs array consist in acquiring pictures of the galaxy clusters in order to identify the weak gravitational lensing phenomena.
Information on the CCD name and producer are reported in Table 2.12.

The exposure time

In order to define the mean exposure time to acquire an image through the visible detectors a brief study has been performed. The purpose of this section is to explain how the SNR of the CCD has been obtained, identifying the limiting time needed by the hitting photons to produce electron without reaching the saturation condition.
The power per unit surface area emitted by the Sun, in a given wavelength range, is the integral of the spectral exitance:

$$\frac{P}{A} = \int_{\lambda_1}^{\lambda_2} \frac{2\pi hc^2}{\lambda^5} \frac{1}{e^{\frac{hc}{\lambda kT}} - 1} d\lambda$$

where h is the Planck's constant, c the speed of light, k the Boltzmann's constant, T the surface temperature of the Sun and A the surface area of the sun. The number of photons produced per unit surface area and unit time is found by dividing the above expression by the energy of a photon:

$$E_\lambda = \frac{hc}{\lambda}$$

obtaining:

$$ph'_0 = \int_{\lambda_1}^{\lambda_2} \frac{2\pi c}{\lambda^4} \frac{1}{e^{\frac{hc}{\lambda kT}} - 1} d\lambda$$

Thus, the number of photons per unit area reaching the Earth each second is easily recovered:

$$ph'_{1AU} = \frac{R^2}{r^2} \int_{\lambda_1}^{\lambda_2} \frac{2\pi c}{\lambda^4} \frac{1}{e^{\frac{hc}{\lambda kT}} - 1} d\lambda$$

where R is the radius of the Sun and r the Sun-Earth distance. Now, it is possible to exploit the definition of apparent magnitude to find the number of photons per unit area and unit time coming from a source of magnitude M:

$$ph' = ph'_{1AU} \times 10^{\frac{M_0 - M}{2.5}}$$

where M_0 is the apparent magnitude of the sun.
The number of photons, although, are not as important as the number of electrons produced are. To find them, the quantum efficiency must be introduced and, since it is a function of λ, its expression must be introduced into the integral:

$$e^-_{1AU} = \frac{R^2}{r^2} \int_{\lambda_1}^{\lambda_2} \frac{2\pi c}{\lambda^4} \frac{QE(\lambda)}{e^{\frac{hc}{\lambda kT}} - 1} d\lambda$$

Thus, the number of electrons produced on the CCD each second is:

$$e^- = e^-_{1AU} \times 10^{\frac{M_0 - M}{2.5}} \times A \times F_{MTF} \times T_p \times T_m$$

where A is the area of the telescope, $F_{MTF} = 0.7$ the spread light across multiple pixels, $T_p = 0.9$ the transparency and $T_m = 0.85$ the transmissivity. The data sheet of the Deep Depletion silicon Astro Multi-2 is reported in table 2.13.

Wavelength (nm)	350	400	500	650	900
QE (%)	30	75	75	80	50

Table 2.13: Deep Depletion silicon Astro Multi-2

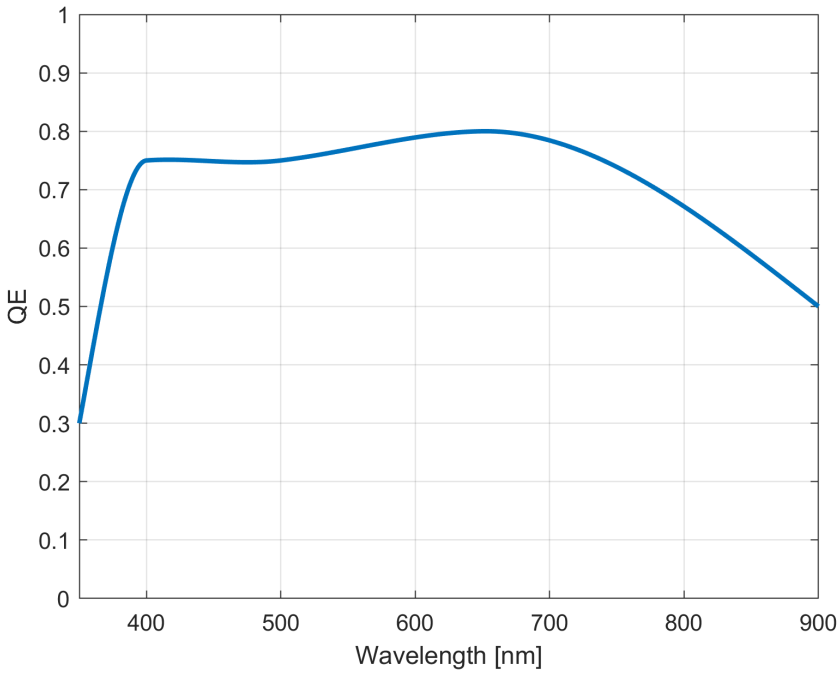

Figure 2.26: Typical QE at -100°C for DD silicon

Figure 2.26 shows an interpolation using the MATLAB `interp1` subroutine.

Knowing that the pixel size is 0.15 arcsec and assuming 0.5 arcmin×0.5 arcmin as mean galaxy size, the number of pixels ($npix$) involved for each galaxy is approximately 40 000 pixels.

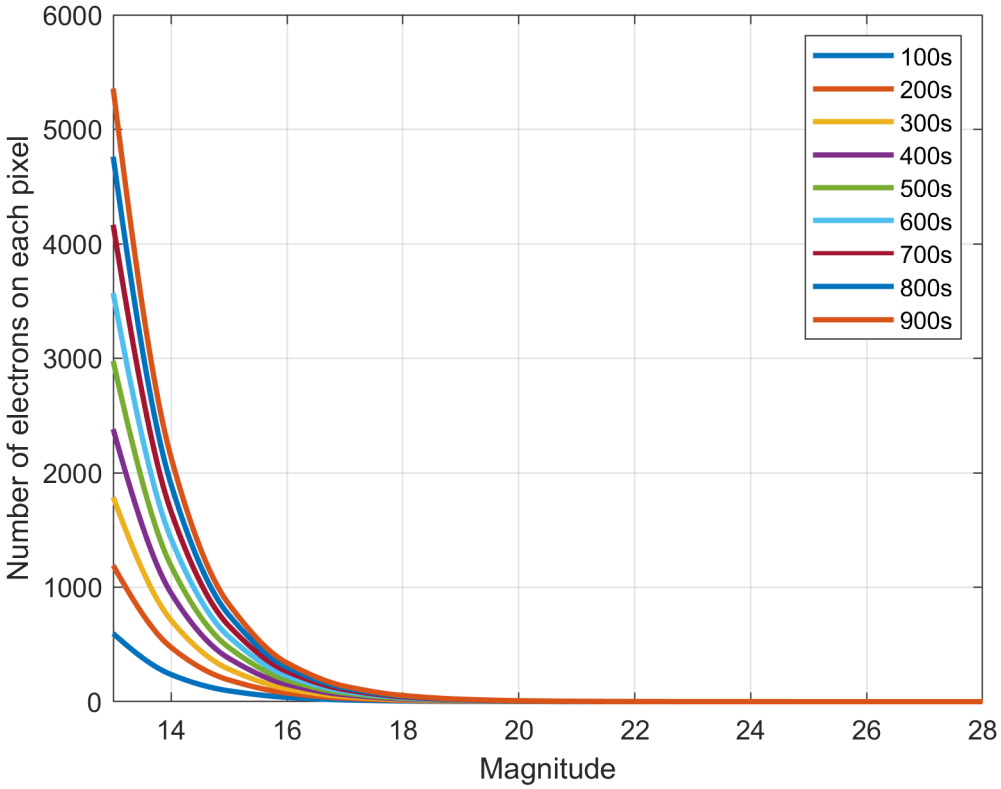

Figure 2.27: Electrons to magnitude and exposure time

Figure 2.27 shows that the number of electrons produced is very high for common objects, i.e. objects with magnitude between 13 and 15, but still far from saturation (350 000 e^-/pixel). The signal-to-noise ratio is computed as:

$$SNR = \frac{G \cdot E \cdot npix}{\sqrt{(F^2 \cdot G \cdot (E + D \cdot t_{exp})) \cdot npix + \sigma_{RON}^2 + \sigma_{QN}^2}}$$

where $E = \frac{e^- t_{exp}}{npix}$ is the electron flux on each pixel, $F = \sqrt{2}$ the excess noise factor, D the dark current produced at a temperature of 173 K, t_{exp} the exposure time, σ_{RON} the read-out noise obtained at 500 kHz read-out frequency, σ_{QN} the quantization noise considering an A/D converter with 16 bit and G the gain. The figure 2.28 shows the SNR for magnitudes between 24 and 28, i.e for the faintest objects, for different exposure time and gain $G = 20$.

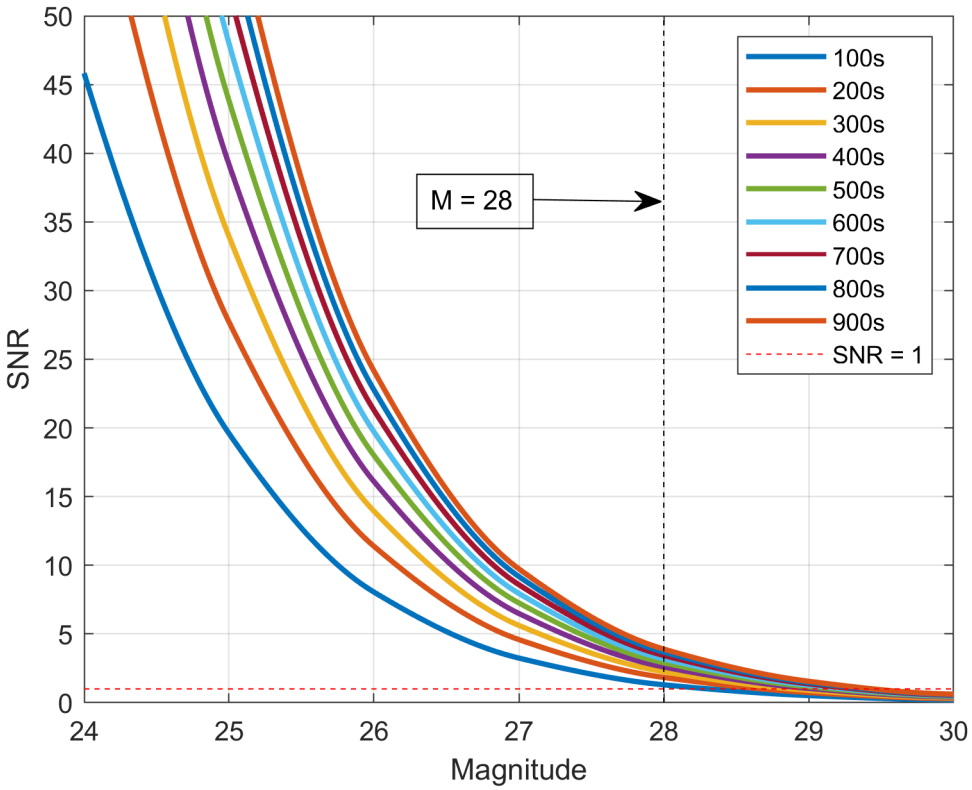

Figure 2.28: Signal to noise

Increasing the exposure time will bring to higher signal-to-noise ratio and more detailed images. Although, it has the disadvantage that the attitude control system must maintain the same pointing accuracy for a longer time. Another increased source of error are the cosmic rays. Indeed, they can produce extraneous bright dots in the image, typically limited to a few number of pixels for short exposure time and easily identified. Selecting $t_{exp} = 900\,\text{s}$, an object with $M = 28$ has a $SNR = 3.90$.

2.2.5 NIR detector: Spectrometer architecture

Two types of spectrometer have been considered for the collection of the data on the infrared spectrum:

- Long slit spectrometer (Baseline)
- Slitless spectrometer (Backup)

Design process description

The scope of the mission is to acquire information on dark matter and dark energy through the observation of distant galaxies and galaxy clusters. As already said, the only way to acquire information on this subjects is to study the effects that they have on the visible matter, since both dark matter and dark energy do not emit any kind of radiation. One of the ways in which they can be studied is by observing the velocity of galaxy clusters and the angular velocity of the stars inside galaxies. With this information, scientists can see the gravitational effects and the energy effects that dark energy and dark matter have on the visible universe. The velocities of far objects is calculated through the red-shift of the spectral lines of some chemical elements that are present in the stars. So a spectrometer is needed on board of the payload to produce this observations. Before designing the architecture of the spectrometer a choice between the different kind of techniques that the detector can use has to be made. For infrared detection the main difference between the various techniques is the slit aperture. This slit is critical to the spectrometer's performance and determines the amount of light (photon flux) that enters the optical bench, and is a driving force when determining the spectral resolution. Four main techniques can be distinguished:

- Single-slit spectroscopy
- Multi-slit spectroscopy
- Slit-less spectroscopy
- Long-slit spectroscopy

The **single-slit spectroscopy** uses a single point slit aperture to select the light that enters in the optical bench. With this technique only the spectral information is acquired and, since the objective is to study also the relative velocities between different points inside galaxies, cannot be used for the mission.

The **multi-slit spectroscopy** uses as slits different apertures located on the FOV. This would be an optimal solution for the measurements that the mission requires but, unfortunately, is not applicable. In fact this technique uses as slit some pre-fabricated masks that have carved on them the slit apertures in optimized places chosen to observe known pre-defined objects. The requirement of the mission is to observe a large amount of clusters and galaxies so a large amount of different masks would be needed on-board the spacecraft. Moreover the geometry of the objects that the telescope needs to observe may not be known. An alternative method to do this kind of spectroscopy uses, instead of a mask, some moving optical fibres. This fibres are placed at each observation in different position, in order to study the object of interest. However

the mechanical structure needed to apply this method is really complex and easily subjected to failure. For all this reason the multi-slit methodology is discharged as a possible solution.

The **slit-less spectroscopy** is a technique that does not use any kind of slit aperture to do the measurement. This kind of spectroscopy works better in scarcely dense regions and divide every point in his spectrum. The position, the dimension and the geometry of the observed object define the aperture in analogy with the slit spectroscopy. Since there is not a slit, there are no slit losses but the resolution cannot be controlled. This technique can be a solution for the mission but not an optimal one. Information on the velocity of the galaxy cluster can be obtained but since the resolution is not something that is adjustable, information on the angular velocity of the galaxies may be lost. For this reasons this technique has been selected as a backup solution.

The **long-slit spectroscopy** is used to observe elongated object and uses as aperture an elongated slit. This technique causes the red-shift to manifest itself as a spatial distribution. In fact, with an elongated slit it is possible to acquire simultaneously spacial and spectral information. Alongside the length of the slit spatial information is acquired while the width of the slit determine the spectral data that is acquired. This is the optimal solution for the science mission, as the telescope needs to study the red-shift of galaxies that are usually elongated objects. Therefore the long-slit spectroscopy has been chosen as a baseline solution for the spectrometer on board of Zwicky.

Long slit spectrometer (Baseline solution)

To define the architecture of the spectrometer first some properties of the objects that the telescope has to observe are needed, such as the wavelength that the instrument needs to cover and the spectral definition needed to see the red-shift effect.
For distant galaxies the angular velocity is studied by looking at the red-shift of the spectral line of the oxygen. The wave length that the detector has to cover goes from the length of the O II of 0.9317 µm to the the one of the O III of 1.6523 µm.
To select the spectral resolution, is here recalled that the red-shift is caused by the Doppler effect. To find the spectral definition needed to appreciate this effect, the following simple equation can be used:

$$\Delta\lambda/\lambda_0 = v_o/c$$

Where $\Delta\lambda$ is the spectral definition, λ_0 is the wavelength of the observed object, v_0 is the velocity of the observed object and c is the speed of light. To select the resolution, the worst possible observable scenario is taken into account, which is the one with the lowest frequency and the lowest velocity of the object, and calculation are made for that case. Knowing that there is a probability of less then 5 per cent of finding a cluster with a one dimensional velocity grater than 600 km/s or lower than 300 km/s, for the study $v_0 = 300$ km/s is taken. As for the frequency the lowest observable one, so $\lambda_0 = 0.9$ µm, is taken. Knowing that the speed of light is 299 792 458 m/s a $\Delta\lambda$ of 0.9 nm is found, the spectral resolution chosen has to be at least half of this value so as a resolution $\Delta\lambda_r = 0.35$ nm is taken.
A long-slit spectroscopy is used, so, in the end an array of detector, one beside the other, is

needed to obtain also the spacial information. First, however, to design the architecture of the single detector and the slit width needed, some observations must be done. After the slit aperture, a diffraction grating is needed to diffract the light in the various region of interest. A grating is chosen over a simple prism because the former can spread the light over a larger angle, granting higher spectral resolution. Also the prism is not an optimal solution for the NIR detection, the glass of which it is made is clear to visible light but it absorbs and blocks ultraviolet and infrared radiation. The grating used is the PCG-1250-10XX-924 that has a central wavelength of operation of 1.064 µm and a grating resolution (G) of 1250 lines/mm. The spectrometer shall also have a collimating and focusing lens before the detector. With the information on the diffraction grating and on the spectral resolution the slit width can be computed. In reality an assumption on the dimension of the detector must also be done: if high resolution is needed (as in this case) a wide detector must be considered. The typical width of $L_d = 25.8$ mm is selected.
Moreover, thanks to the definition of the resolution in the spectrum, the number of pixel needed to do the measurement can be found. Because the frequency between $\lambda_m = 0.9$ µm and $\lambda_M = 1.7$ µm are the one of interest for the mission, the number of pixels for one detector can be found as:

$$(\lambda_M - \lambda_m)/\Delta\lambda_r = 2286 \text{ pixels}$$

With the following equations the width of the slit is computed:

$$\alpha = (\arcsin \frac{\lambda_c G}{2\cos\Phi/2})\frac{\Phi}{2}$$

$$\beta = \Phi - \alpha$$

$$L_f = \frac{L_d \cos\beta}{G(\lambda_M - \lambda_m)}$$

$$L_c = L_f \frac{\cos\alpha}{M\cos\beta}$$

$$w_s = \frac{G\Delta\lambda_g L_c}{\cos\alpha} = 8 \text{ µm}$$

Where $\lambda_c = (\lambda_M - \lambda_m)/2$, α and β are respectively the incidence and diffraction angle of the grating and the chosen configuration is the classical one that has $\alpha = -\beta$, L_c is the focal length of the collimating lens, L_f is the focal length of the focusing lens and M is a selected magnitude of 1. The dimension of the pixel in the spectrum can be found as:

$$L_d/2286 = 12 \text{ µm}$$

The kind of detector that is chosen after all these considerations, is the linear InGaAs (indium gallium arsenide). This family of detectors are of the intrinsic and photo-voltaic type, they have a spectral response in the range of the 0.9 µm to 1.7 µm, an operating temperature of 300 K and a typical acquisition rate of 350 Hz.

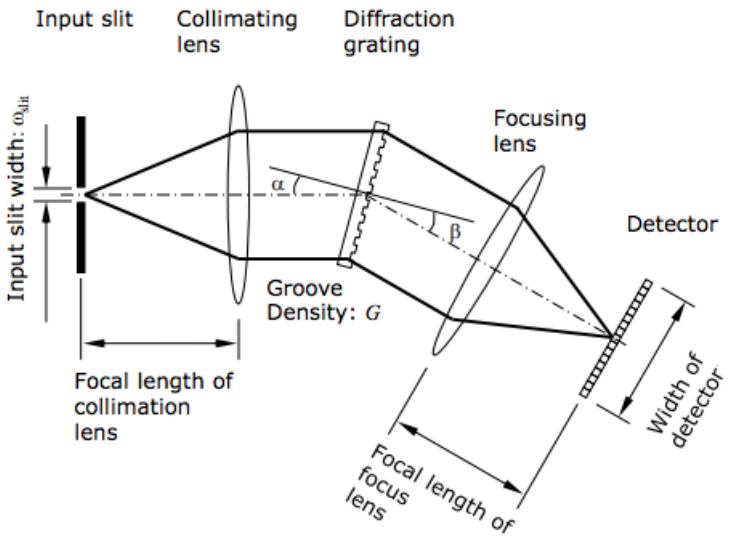

Figure 2.29: Architecture of the spectrometer

Until now, considerations have been made on a singular spectrometer only. In order to perform the long-slit spectroscopy, multiple detectors, one beside the other, are needed. An array of detectors, and not a single huge detector, must be present for reason of redundancy. In fact, in the latter case the failure of the detector will prevent the telescope from doing any kind of data acquisition in the NIR, while in the array situation, with the failure of one detector only, just one line of the image would be lost.
Now, in order to dimension the length of the slit, the numbers of detectors and the dimension of the pixel in the spacial dimension, some consideration on the resolution of the image in the infrared has to be done. From the optical sensor architecture definition has been found that, with the chosen aperture diameter, the resolution in the NIR is of 0.2 arc-seconds. Knowing that the pixel needs to have a FOV at least double the resolution granted by the telescope, a $\theta_fov = 0.4$ arcsec is selected. Using again the equation viewed in the optical design, the computation of the pixel radius of the spectrometer can be done:

$$r_d = tan(\theta_{fov}/2) * f = 19\,\mu m$$

where f is the equivalent focal length of 19.9328 m.
Therefore, the diameter of the pixel is 38 µm. The pixels in the detector are in this way rectangular, of dimensions 38 µm $\times$12 µm. From the Abell catalog it can be seen that the dimensions of the galaxies in distant galaxy clusters can go up to some seconds. As consequence a selection of an array of 12 detectors is made. With this selection a line in the FOV is 0.4 arcsec width and 4.7 arcsec long. To have an appreciable measure of the angular velocity inside the galaxy, at least 4 pixels of spatial information are needed, so if there are galaxies smaller than 1.6 arcsec in diameter, the spectrometer cannot provide enough data to extrapolate the information. With the number of detectors and the pixel size, the length of the slit is finally defined as $l_s = N_d * d_d = 456\,\mu m$, where N_d is the number of detectors and d_d is the diameter

of the pixels. A single spectrometer of this kind has a mass of 0.0156 g, so the total mass of the instrument is $m_d = 0.187\,\mathrm{g}$
A summary of all the proprieties of the spectrometer seen is shown in table 2.14. The agency to which the construction of the spectrometer has been commissioned is the **Ibsen Photonics**.

Slit Width	$w_d = 8\,\mu\mathrm{m}$
Slit Length	$l_d = 456\,\mu\mathrm{m}$
Type of detector	InGaAs
Grating	PCG-1250-10XX-924
Acquisition Frequency	$f_d = 350\,\mathrm{Hz}$
Working Temperature	$T_d = 300\,\mathrm{K}$
Number of pixel per detector	$N_d = 2286$
Number of detectors	$N_d = 12$
Mass of the instrument	$m_d = 0.187\,\mathrm{g}$
Dimension of the pixel	$38\,\mu\mathrm{m} \times 12\,\mu\mathrm{m}$
Spectral range	$0.9\,\mu\mathrm{m} to 1.7\,\mu\mathrm{m}$
Spectral definition	$\Delta\lambda_r = 0.35\,\mathrm{nm}$
Width of the spectrometer	$h = 0.258\,\mathrm{m}$

Table 2.14: Long slit spectrometer data

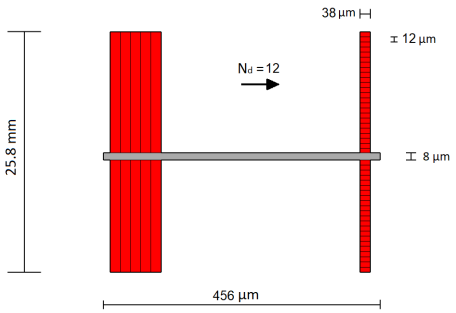

Figure 2.30: Long-slit Spectrometer Scheme

Moving mirror design

With the long-slit spectroscopy, only a line of the entire field of view pass through the slit and is analyzed by the detectors. A way to change the selected light that pass through the aperture must be implemented.
A moving mirror prior to the slit is the selected solution to move the light on the slit. However, a moving mirror alone is not enough. Indeed, rotating it around just one axis, the line seen by the slit moves only in one direction on the FOV. An additional movement is needed to shift the slit in the direction perpendicular to the one granted by the rotation of the mirror. Creating a system that allows the rotation of the moving mirror around two perpendicular axis is not advised because of the complexity of the system and the possibility of failure. What is done instead is allowing the detector to move in the direction perpendicular to the one granted by the rotation of the mirror.
Another auxiliary system of the detector is the photometer. The telescope is observing sparsely populated areas, in the worst case scenario the galaxies occupy only 1/100 of the cluster. The acquisitions done by the spectrometers are not needed on all the FOV but only on the portion containing galaxies, so photometers are installed on-top of the array of detectors, so that the light coming from the moving mirror reaches them first.
The number of photometers needed is the same as the number of detectors and the portion of the FOV that the single photometer has to cover must be the same of the detector's pixel.

If light is detected, the spectrometers has to do the acquisition. With this configuration the scanning of the FOV can be done only in one rotation sense of the mirror because the light must arrive first at the photometers and then at the spectrometers. So, after scanning an entire row, the mirror must return to the initial position before starting the scan of the next row.
With this information, the design of the movement of the mirror can be done. From the mirror sizing, the dimension of the moving mirror is known to be $0.2733 \times 0.2733 \times 0.0011\,\text{m}$.
If the FOV is assumed for simplicity to be squared, we have that every side has a dimension of 0.7 degree, that means 2520 arcsec. With this information the computation of the number of different positions in which the slit must be placed to see all the FOV is done as follows:

$$\frac{2520 * 2520}{4.7 * 0.4} = 3377872$$

Where 0.4 is the portion of the FOV seen by the slit in one dimension and 4.7 is the portion seen in the other. The angle that the moving mirror has to cover is easily computed knowing the distance between the detector and the mirror, and the equivalent width of the FOV (which is the dimension of the focal plane) on the detector. The rotation angle is found to be:

$$\theta_r = 27.12^\circ = 0.473\,\text{rad}$$

A realistic angular velocity of the moving mirror of $\Delta\omega_m = 0.236\,\text{rad/s}$ is imposed, so that a row of the mirror is done in 2 seconds.
The number of rows that the slit has to do is $2520/4.7 = 536$. As already observed, the mirror must return at the starting position at the end of every row, so the time needed with this angular velocity to cover all the FOV is:

$$\Delta t_\omega = 2144\,\text{s}$$

Every time that light is detected by the photometers, the mirror has to stop moving and let the spectrometers do the acquisition. The acquisition frequency of the detectors was already defined so, by studying the worst possible scenario, where the telescope is looking at a relative high populated area, the maximum time needed to cover all the FOV is found. If looking at crowded clusters, the spectrometers need to do acquisitions on 1/100 of the FOV. The time needed to acquire the spectrum of that portion of the sky is:

$$\Delta t_M = \frac{3377872}{f_a * 100} = 96\,\text{s}$$

where f_a is the acquisition frequency of the spectrometers, equal to 350 Hz. When the moving mirror is stopped it also needs to be stabilized on the position in which the spectrometers have to work. Another $\Delta t_s = 0.5 * \Delta t_M$ must be added. Also, a PID controller must be implemented to perform the stabilization.
The total time needed by the spectrometer system to acquire the needed data in the worst case scenario is now computed as:

$$\Delta t_{tot} = 2288\,\text{s}$$

The torque that an electric motor needs to give to the moving mirror is now defined.
The moving mirror is a cuboid of dimension $0.2733 \times 0.3500 \times 0.0110\,\text{m}$ of beryllium that has a

density of $\rho_{Be} = 1848\,\mathrm{kg/m^3}$, so its mass is $m_m = 1.9\,\mathrm{kg}$.
The torque is equal to:

$$C_m = M_m = I_h \times \frac{d\omega}{dt}$$

The moving mirror has to reach almost instantly the ω_m because it has to start scanning the FOV with the needed speed as soon as possible. The time needed to reach the angular velocity is chosen as $dt = 2/6300\ \mathrm{s} = 3.175 \times 10^{-4}\,\mathrm{s}$, where 6300 is the number of points that the slit has to see in one row.
The value obtained is $C_m = 8.8\,\mathrm{N\,m}$.
A Micro3 Rotary Incremental Actuator is therefore selected and its properties are listed in table 2.15.
Two actuators are implemented in the design for redundancies so that, in case of failure of one of them, the presence of the other still allows the rotation of the mirror.
The crankshaft of the actuator is connected to the moving mirror by a bushing, a pre-load in the connection has to be designed so that the mirror is moving with the crankshaft even in the case of max torque. The friction in the junction is between aluminium and aluminium, so the friction coefficient is $\mu_{Al-Al} = 1.1$ and the pre-loading is computed as:

$$F_{load} = \frac{M_f * \mu_{Al-Al}}{R_{ck}} = 387\,\mathrm{N}$$

where R_{ck} is the radius of the crankshaft of 0.025 m. The F_{load} is oversized to 500 N.

Actuator Name	Micro3 Rotary Incremental Actuator
Output Couple	20 N m
Weight	1.6 kg
Working Temperature	228 K to 358 K
Power Consumption	3 W

Table 2.15: Micro3 Rotary Incremental Actuator Properties

Also the array of detectors needs to move but, once it reaches the end of stroke, it does not need to return in the initial position to start doing acquisitions again. For the next picture the instrument will simply move in the opposite direction with respect to the previous one. The length of the trail on which the detectors are allowed to move must be of 0.25 m, which is a bit more of the length of the focal plane. While the mirror is doing the returning maneuver, the array of detectors needs to move of 456 µm, so the force that the actuator needs to give is:

$$F_a = a_d * m_d$$

with a_d the acceleration of the array that is computed as:

$$a_d = \frac{\frac{456\times10^{-6}\ m}{2\ s}}{2\ s} = 1.14 \times 10^{-4}\,\mathrm{m\,s^{-2}}$$

The value obtained is $F_a = 2.1318 \times 10^{-5}\,\mathrm{N}$
A SLL12 nanometer precision linear rail positioner is selected and its properties are listed in table 2.16. The mass of the actuator with the length that the spectrometers need to cover is $m_{act} = 0.144\,\mathrm{kg}$.

Actuator Name	SLL12
Movement Precision	1 µm
Trail Weight	59 g/100 mm
Rail length	70 mm to 475 mm
Max Lift Force	1 N
Weight	0.144 kg
Working Temperature	242 K to 372 K
Power Consumption	2 W

Table 2.16: SLL12 Properties

Slitless spectrometer (Backup solution)

As seen in the introduction to the selection of the spectrometer, for the backup solution the slit-less spectroscopy technique has been selected.
This kind of spectroscopy does not require any kind of slit aperture and the resolution of the image is given by the position, the geometry and the dimension of the observed objects.
In fact, in analogy with the slit case, the aperture is given by the observed object itself (for the galaxies, or more generally for non circular objects, the semi-major axes defines a virtual inclined aperture).
The absence of a slit means that a selection of the photon flux is not needed, so there is not the need of a moving mirror before the spectrometer. This also means that the acquisition of the FOV is done all at the same time also in the NIR and not only in the visible light. An array of spectrometers that covers all the FOV is required but without the necessity of the moving actuator.
This kind of spectroscopy works better in scarcely dense areas, as the one observed by the telescope, but as already noted, that there is no control over resolution and the spectral line of different objects can overlap. In fact, since the position of the apertures depends on the object position in the sky, the spectral overlapping often happens.
There must be also in this case a grating for the light diffraction and even the photometers are needed.
As position and geometry of the observed object are not so well defined with the photometers, it is possible to extrapolate better this information and the process can be automatized.
To summarize, this technique is simpler respect to the long-slit spectroscopy because it requires less mechanical elements and is proven to be working in space (it has been used in missions like the EUCLID mission and on the CRASSLEY telescope).
However by using this method there are more contamination effects, a loss of resolution and, as a consequence, a possible loss of important information like the angular velocity of the galaxies.

Figure 2.31: Example of spectral overlap in slit-less spectroscopy

2.2.6 Data Compression

Due to the huge amount of scientific data acquired by the two detectors and the short time window to communicate with the ground segment, lossless data compression is necessary in order to increase the science return and to reduce the requirement for station contact time, and data archival volume.
As data must be compressed, but the original quality must be retained, only lossless compression techniques has been investigated.
A lossless compression technique guarantees full reconstruction of the original data without incurring any distortion in the process.
A lossless data compression technique preserves the accuracy of the source data by removing redundancy from the source data itself, generating a compressed version of the original file. During the decompression process the original source data is reconstructed from the compressed file by restoring the removed redundancy. The quantity of redundancy removed from the source data is variable and is highly dependent on the kind of source data that shall be compressed.
After compression has been performed, the resulting variable-length data structure can be packetized and sent over the space-to-ground communication channel in a way that enables the ground system to recover the data with high reliability. The contents of the packets are then extracted and their data units are provided to the ground sink in sequence to be decompressed.
It must be also observed that packetization is essential to mitigate the possibility of error propagation in the event of a bit error, which can lead to a reconstruction error over successive data points during the decoding of the information.
A good compression algorithm, which can be implemented on-board, should satisfy the following criteria:

1. The algorithm has to adapt to the changes in data statistics to maximize performance
2. It can be easily implemented with few processing steps, small memory and little power

3. It can be easily interfaced with a packetized data system without requiring a priori information or re-establishing data statistics for every packet
4. In case of bit error in the data stream, the decompression error can be contained in individual packet

Lossless data compression techniques such as zip, gzip and winzip are widely used for compressing files residing on PCs.
These techniques are all based on the Lampel-Ziv-Welch algorithm or its variations, and would generally yield poor compression ratios on data originating from spacecraft instruments.
For what concerns space applications, the Consultative Committee on Space Data Systems has recommended two lossless compression algorithms, which will be briefly described in the next subsections.

The Discrete Wavelet Transform

The basic idea of the wavelet transform is to represent an arbitrary function $f(x)$ as a linear combination of a set of such wavelets or basis functions. These basis functions are obtained from a single prototype wavelet called the mother wavelet by dilations (scaling) and translations (shifts). Compared to Windowed Fourier analysis, a mother wavelet is stretched or compressed to change the size of the window. In this way, big wavelets give an approximate image of the signal, while smaller and smaller wavelets zoom in on details. Therefore, wavelets automatically adapt to both the high-frequency and the low-frequency components of a signal by different sizes of windows. Any small change in the wavelet representation produces a correspondingly small change in the original signal, which means local mistakes will not influence the entire transformation.
The main purpose of wavelet transform is to change the data from time-space domain to time-frequency domain which makes better compression results.
For Zwicky purposes, the DWT can be employed to encode the data generated by the CCD array, in order to reduce the size of the science related information that shall be sent back to the ground station and in turn reduce the required downlink data rate.
Implementation of the DWT for space applications is more detailed in reference [23].

The Rice Algorithm

A study conducted by NASA [17] identified in the Rice compression algorithm a good trade off between the four statements that a good compression algorithm should satisfy.
A block diagram of the architecture of the Rice algorithm can be seen in figure 2.32 (taken from [22]):

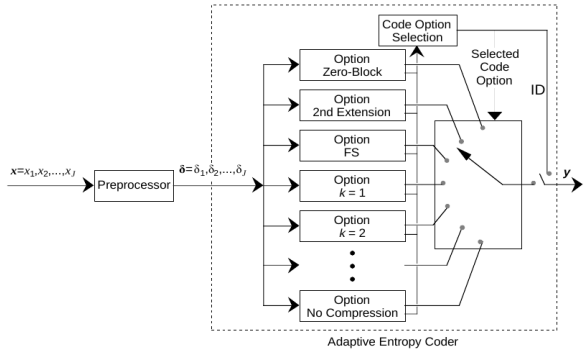

Figure 2.32: Rice Encoder Architecture

As it can be seen, it consists of a preprocessor to decorrelate data samples and subsequently map them into symbols suitable for the entropy coding stage. To ensure that compression is lossless, the preprocessor must be reversible.
The input data to the preprocessor, x, is a J-sample block of n-bit samples. The outputs of the prepocessor are then block of preprocessed samples δ, wich then are given to the adaptive entropy coder. The adaptive entropy coder then gives the encoded bit sequence y. The adaptive entropy coding block has a collection of different variable-length coding option which can be applied to each block of the J preprocessed samples, in order to archive the best compression for each block.
Each encoded block is preceded by an ID bit pattern that identifies the coding option to allow the decoder to correctly decode the block itself.
At the ground segment the encoded signal can be decoded by the lossless decoder, which consists of two separate functional parts, the post-processor and the adaptive entropy decoder, as can be seen from the figure 2.33 (taken from [22]):

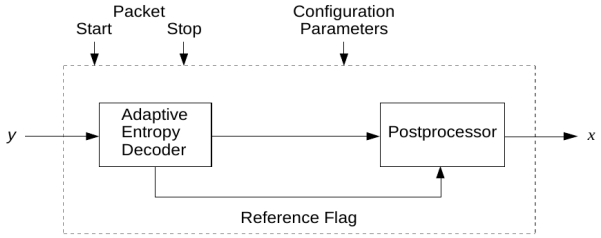

Figure 2.33: Rice Encoder Architecture

The postprocessor performs both the inverse prediction operation and the inverse of the standard mapper operation. The configuration parameter of the decoder must match those of the encoder, so both of them will operate in the same mode. The inputs to the decoder are:

- the source packet data field containing the compressed source data y
- the source packet data field start and stop signals
- the decoder configuration parameters

The decoder configuration parameters are needed in order to process the compressed variable-length data contained within the source packet data field.
The compression ration CR is defined as the ration of the number of bits before the compression to the encoded data rate [22]:

$$CR = \frac{nJ}{average\ CDS\ length\ in\ bit}$$

where n is the sample resolution, J is the block size and CDS stands for Coded Data Set.
For imaging purposes, CR can reach values up to 5 or even more with high level of thresholding, when using the Rice algorithm [18].
For non imaging purposes, Rice algorithm can reach values of CR up to 26 [18].
The value of CR clearly depends on the specific instruments which acquire the source and from the entropy level of the data that should be encoded.
For Zwicky purposes, the Rice algorithm can be employed to encode the data which comes from the spectrometers array, in order to reduce the size of the science related information that shall be sent back to the ground station and in turn reduce the required downlink data rate.
Implementation of the Rice algorithm for space applications is more detailed in reference [22].

2.2.7 On-board data handling architecture

Due to the large on board data processing load required by Zwicky, the Payload Data Handling Subsystem has a decentralized architecture, as it can be seen in figure 2.34:

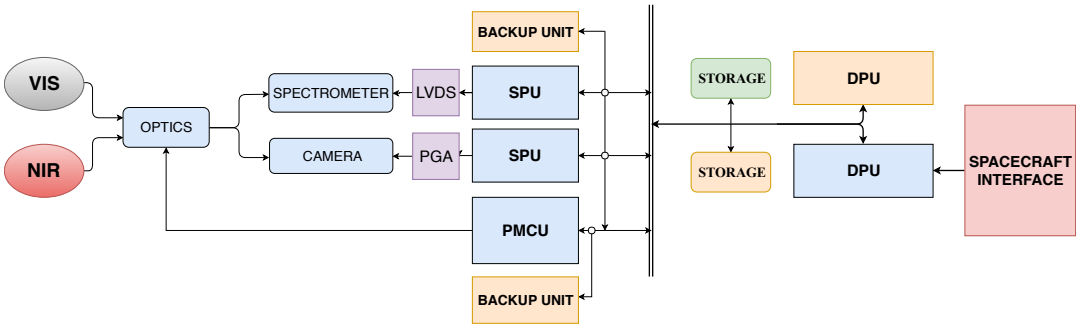

Figure 2.34: Payload Data Handling Subsystem architecture

The Data Processing Unit is the interface between the payload instruments and the S/C OBDH, while each instrument will be connected to a Science Processing Unit and a Compressor.
The Data Processing Unit is the central core of the PDHS and drives the two Science Processing Unit plus the Payload Mechanism Control Unit.
The Data Processing Unit (DPU) shall send telecommands to the Science Processing Unit (SPU), and collect information about the health status of the payload instruments and perform housekeeping tasks. The DPU is directly connected with the S/C OBDH trough the SpaceWire protocol to perform several tasks among which:

- send science data from the Storage Unit to the S/C OBDH

- inform the S/C OBDH about the health status of payload's instruments
- receive from S/C OBDH telecommands sent by the ground segment to the PDHS

The DPU will also contain the software implementation of the operating modes described in section 2.4.3.
As said before, Zwicky is equipped with two science processing units.
One SPU is connected to the CCDs array, while the other one is connected to the spectrometers array.
The SPU are responsible of interfacing the detectors with the readout electronics, and command the data acquisition sequence.
Once the acquisition of a sequence is completed the source data is saved to the storage.
During the next exposure time the SPU shall retrieve and send the acquired data to the compressor stage that performs the compression.
The output files of the compressor will then be sent back to the SPU and stored into a dedicated directory inside the on-board storage unit.
The SPU will also be responsible of the acquired data matching with the S/C telemetry.
The moving part of the optical telescope instead will be managed through a micro-controller, namely the Payload Mechanism Control Unit, driven by the DPU.
A simplified scheme of the PDHS can be seen in figure 2.35:

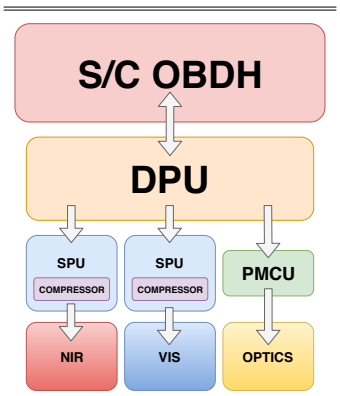

Figure 2.35: Payload Data Handling Subsystem

2.2.8 Power Bus

In order to power up all the components of the payload, a power control unit is present (fig 2.37).
The PCU distribute the power across all subsystems, providing each device the correct voltage and current, according to the power bus architecture shown in figure 2.36.

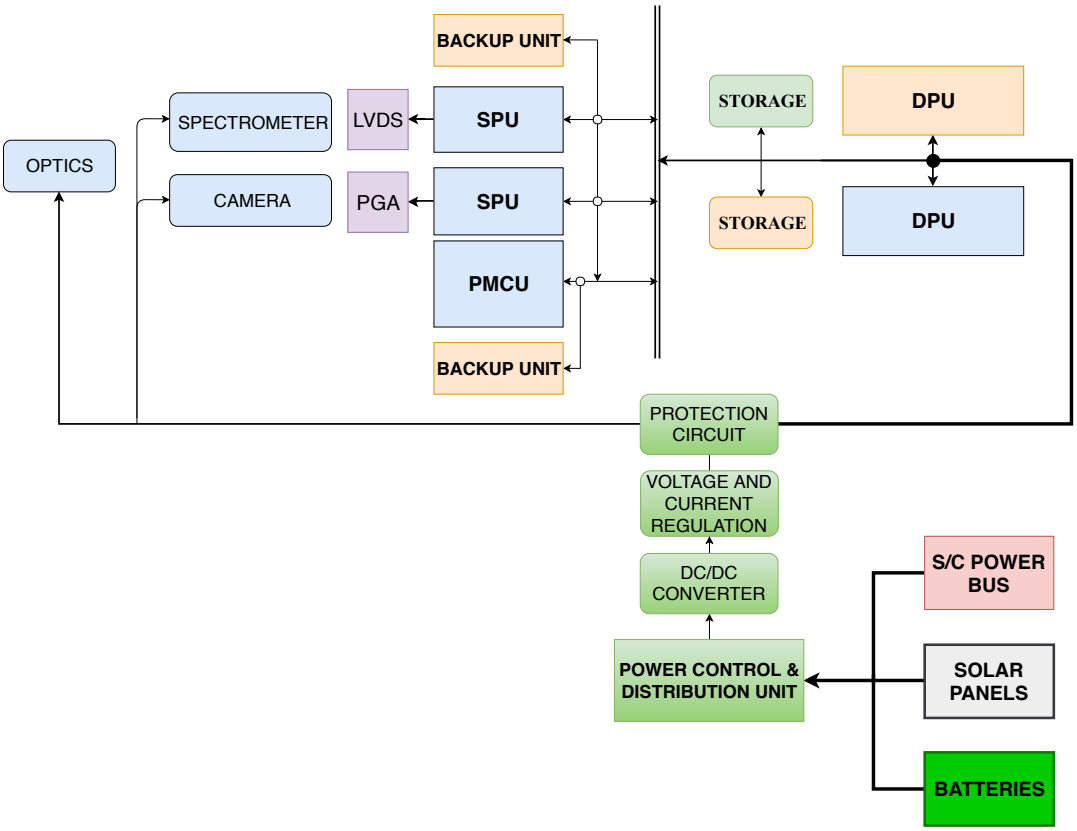

Figure 2.36: Power Bus architecture

The PCU integrates also a protection circuit to avoid possible failures of the connected devices due to overvolting or overcurrent.

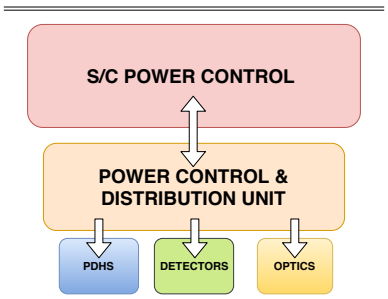

Figure 2.37: Power Control and Distribution Unit

The overall architecture of the payload data handling subsystem and the power bus is shown in figure 2.38:

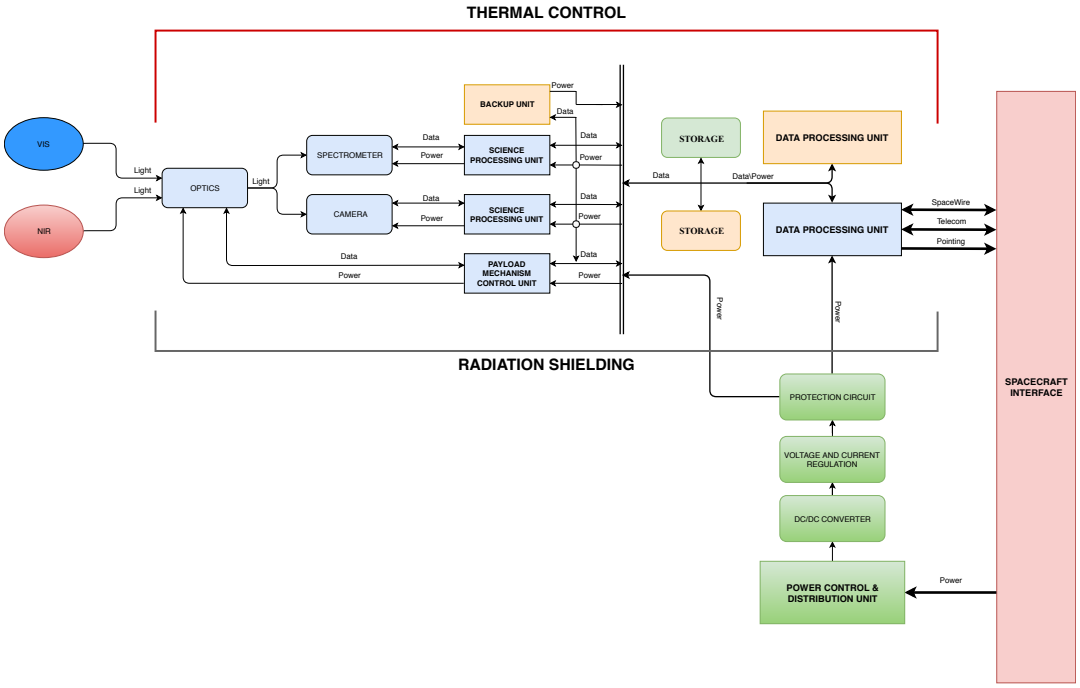

Figure 2.38: Functional Scheme of PDHS + PCS

where it is also indicated that electrical components shall be shielded against radiation and be thermally controlled.

2.3 System Description

2.3.1 Launch Vehicle

The mission objectives concerning the operating environment impose to choose a launcher that can perform an orbital transfer to reach the HEO chosen for the achievement of the mission.
The chosen launcher for the mission is the ARIANE 6 A64, provided by ARIANESPACE, and will be launched from the Guiana Space Centre in 2025.
The disturbance loads provided by the launcher can be sub-divided into two main groups:

- Static loads
- Non static loads

The following incoming loads must be taken into account in order to verify the stability of the structure.

Static loads

Zwicky and the spacecraft will experience static loads during ground operation and during the flight.
The main values of the static loads will be expressed in terms of acceleration along the main directions are:

- Longitudinal
- Lateral

Acceleration (g) / Critical flight events	Longitudinal		Lateral
	Static	Dynamic	Static + Dynamic
Lift-Off	-2	± 1.5	± 2
Aerodynamic phase	-2.8	± 0.8	± 2
Pressure oscillations	-4.6	± 1.4	± 1
ESR jettisoning	-0.9	± 3.1	± 0.9
LLPM	-2.9	± 1.4	± 0.5
ULPM	-3.1	± 1.4	± 0.5

LLPM = Flight between ESR separation and LLPM separation
ULPM = Flight between VINCI ignition and Payload separation
The minus sign with longitudinal axis values indicates compression.
Lateral loads may act in any direction simultaneously with longitudinal loads.
The Quasi-Static Loads (QSL) apply on payload CoG.
The gravity load is included.

Table 2.17: Quasi-Static Loads Flight limit levels for a satellite with a mass between 2000 kg and 3400 kg

Non static loads

As reported from the manual, during the flight non static loads are present, besides the static ones, which are:

- Sinusoidal Loads
- Acoustic Loads

The sinusoidal loads occur mainly during the atmospheric flight and can also occur during transient phases.
The total time duration of these kind of loads is about 6 minutes. The table below indicates all the frequency bands of the sinusoidal loads and each amplitude in terms of acceleration along the principal directions.

Direction	Frequency band (Hz)	Sine amplitude (g)
Longitudinal	2 – 50	1.0
	50 - 100	0.8
Lateral	2 – 25	0.8
	25 – 100	0.6

Table 2.18: Sinusoidal Loads

During flight, acoustic pressure fluctuations under the fairing are generated by engine operation (plume impingement on the pad during lift-off) and by unsteady aerodynamic phenomena during atmospheric flight, which are transmitted through the upper composite structures.
Apart from lift-off and transonic phase, acoustic levels are substantially lower than the values indicated hereafter.

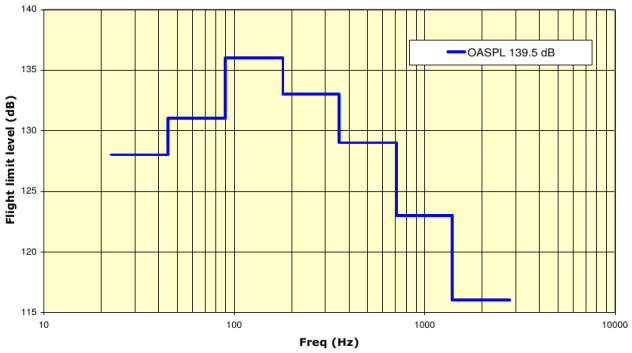

Figure 2.39: Acoustic Loads

In this paper only a static analysis has been performed, taking into account the superposition of the effects reported on the tables 2.17 and 2.18. Thus the maximum static acceleration imposed to the S/C in the longitudinal direction is given by the maximum quasi-static acceleration experienced during the flight, 4.6 g, plus its dynamic component, 1.4 g, plus the maximum value of the sinusoidal component of the load, 1 g. Analogously, the maximum static acceleration imposed in the lateral direction is given by the maximum quasi-static acceleration plus its dynamic component, 2 g, plus the maximum sinusoidal component, 0.8 g. Therefore, the values considered for the simulation are 7 g for the longitudinal direction and 2.8 g for the lateral. Both the accelerations are applied simultaneously and at the center of gravity of the S/C during the simulation. Acoustic loads are not considered in this phase, as the designed kind of structure is not susceptible to these loads.

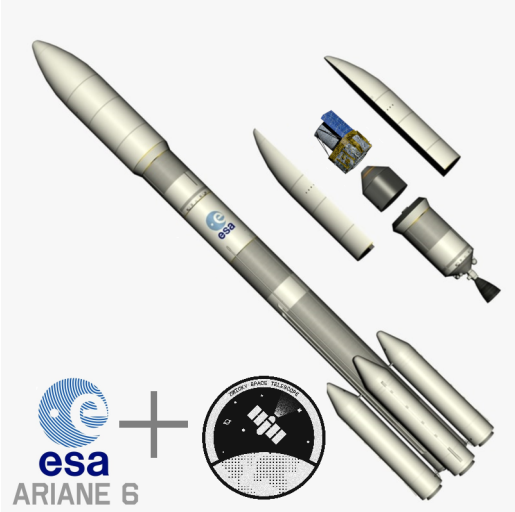

Figure 2.40: Integration of the Zwicky S/C and the Ariane 6 launcher

2.3.2 Spacecraft

Zwicky is an observatory spacecraft composed by one single payload.
Zwicky shall be oriented vertically within the launcher. The gravity center of the spacecraft must stay within a distance of 30 mm from the launcher longitudinal axis and between 750 mm and 3400 mm from the separation plane, as reported on the user manual, in order to ensure static balancing.
The spacecraft shall be designed to have a center of gravity that fits these requirements.

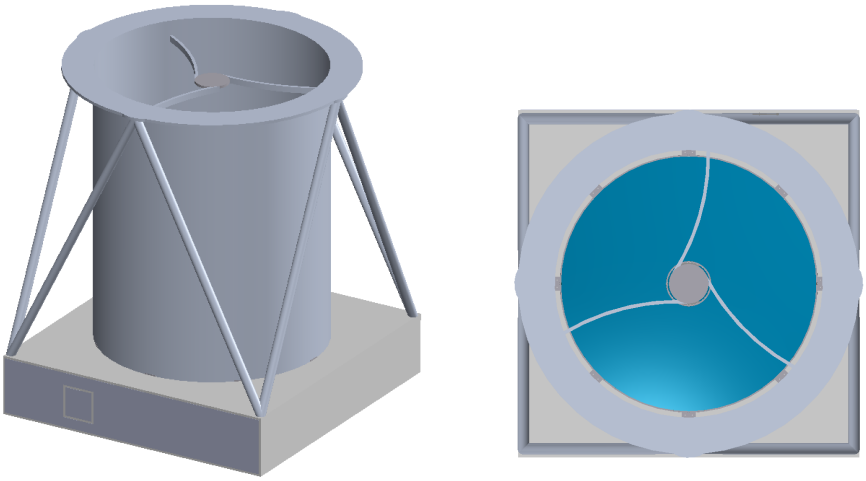

(a) Rendering of the payload (b) Top view

Figure 2.41: Zwicky structure

2.3.3 Structures

Zwicky's components can be divided in two categories: structures designed to act as supports and components chosen to accomplish the mission objecives. This section is dedicated to Zwicky's structures, which are:

- **Hollow cylindrical body**, thick 5 mm, made of aluminium alloy
- **Hollow box**, composed by a sheet of 3 mm and a truss structure, both in aluminum
- **Hollow beams**, to prevent vibrations of the cylinder and with thin a thickness of (2.5 mm) to have high first lateral mode frequency without being too heavy
- **Three curved beams**, to support the secondary mirror and minimize the diffraction, with low upper thickness to maximize the available area for the incoming light
- **Instrument box**, that contains the CCD, the spectrometer, the reflectors and all the supports. Both the box and the little supports are made of aluminum alloy.
- **A lightweight support for the primary mirror** composed by: a circular bottom plate thick 20 mm, made of aluminum alloy, an inner and an outer rings, both 10 mm thick and

made of aluminum alloy, an internal honeycomb structure.
All to support the mirror itself, thick 10 mm and made of SiC (silicon carbide)

- **The supports for the secondary mirror** made of aluminum alloy
- **The supports for the tertiary mirror and all the reflectors** made by properly shaped aluminum alloy.

This preliminary structure definition leaves approximately $0.9\,m^3$ of empty space.

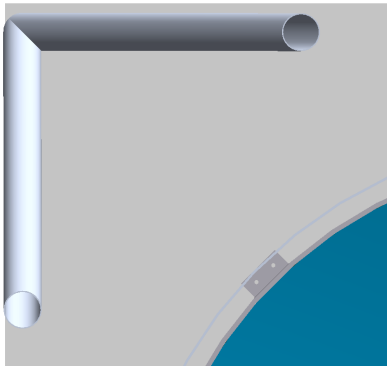

(a) Section of the hollow beams

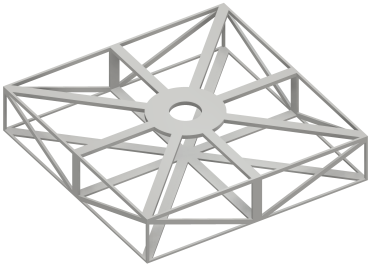

(b) Internal truss of the box

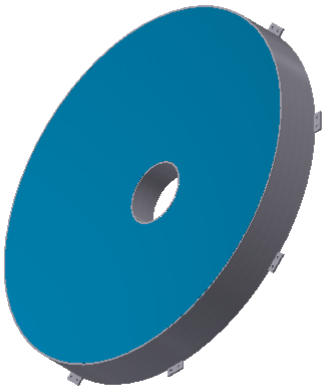

(c) Primary mirror

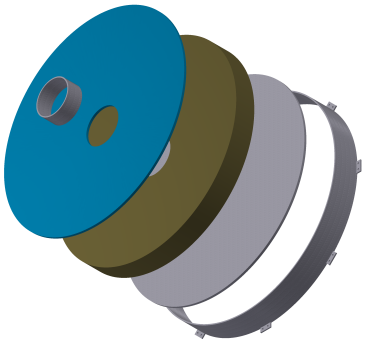

(d) Assembly of the primary mirror

Figure 2.42: Zwicky structural components

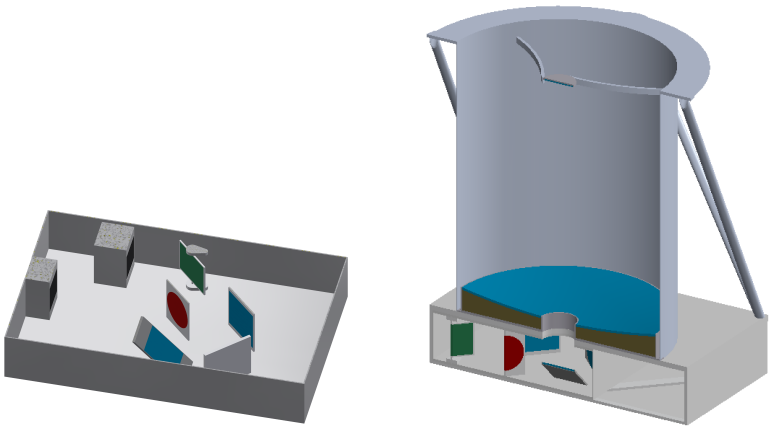

(a) Assembly of the instrumentation inside the box

(b) View of a section

Figure 2.43: Zwicky structure sections

Static structural analysis

ANSYS software has been selected for this analysis. For the static analysis a longitudinal constant load of 7g and a lateral constant load of 2.8g has been considered, due to the consideration written in 2.3.1.
Since the lateral loads act on a plane, a single direction for the simulation must be chosen. The best choice would be to detect the weakest axis.
In the analysis two option has been considered, a direction parallel to the weakest principal axis (X axis in the figures) and one parallel to the diagonal of the top face of the box. The biggest maximum deformation is observed in the second option, with a difference of approximately 3%.
The payload is fixed at the base.
Even if this analysis has more rigid conditions than the real launch (since in the launcher the maximal load is applied only for a short period of time), the results are positive, with a maximum stress of about 2.2×10^7 Pa and a maximum elastic deformations of small magnitude (in the order of 1×10^{-4} m).
All the deformations are in the elastic field.
This means that the structure satisfies the static requirements of the launcher.

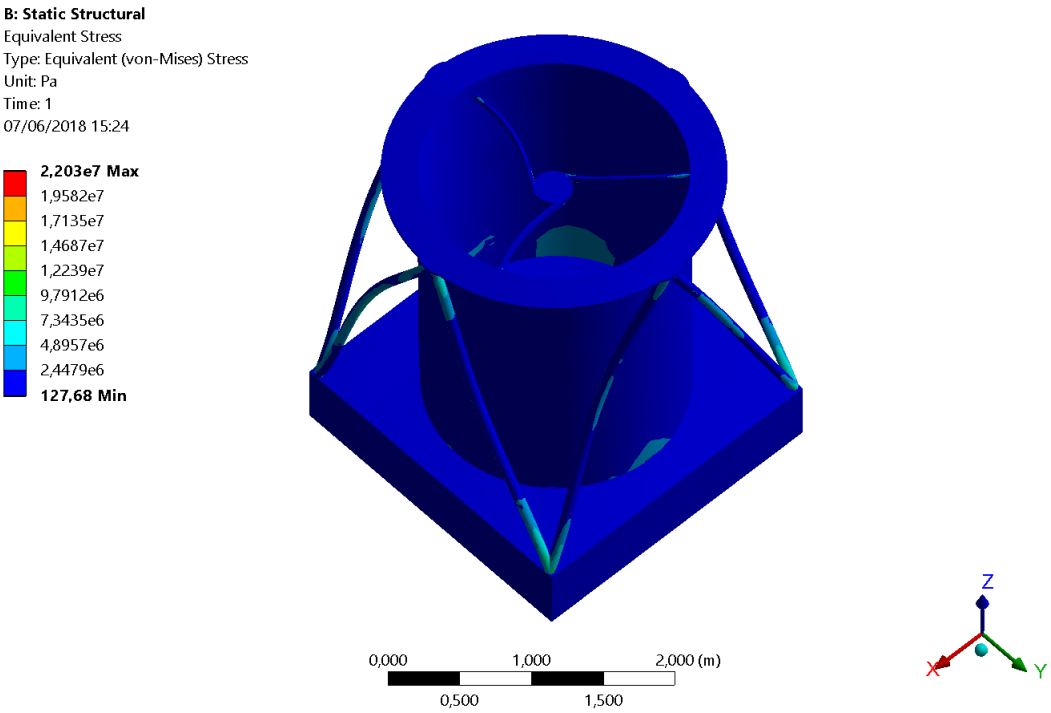

Figure 2.44: Equivalent stress

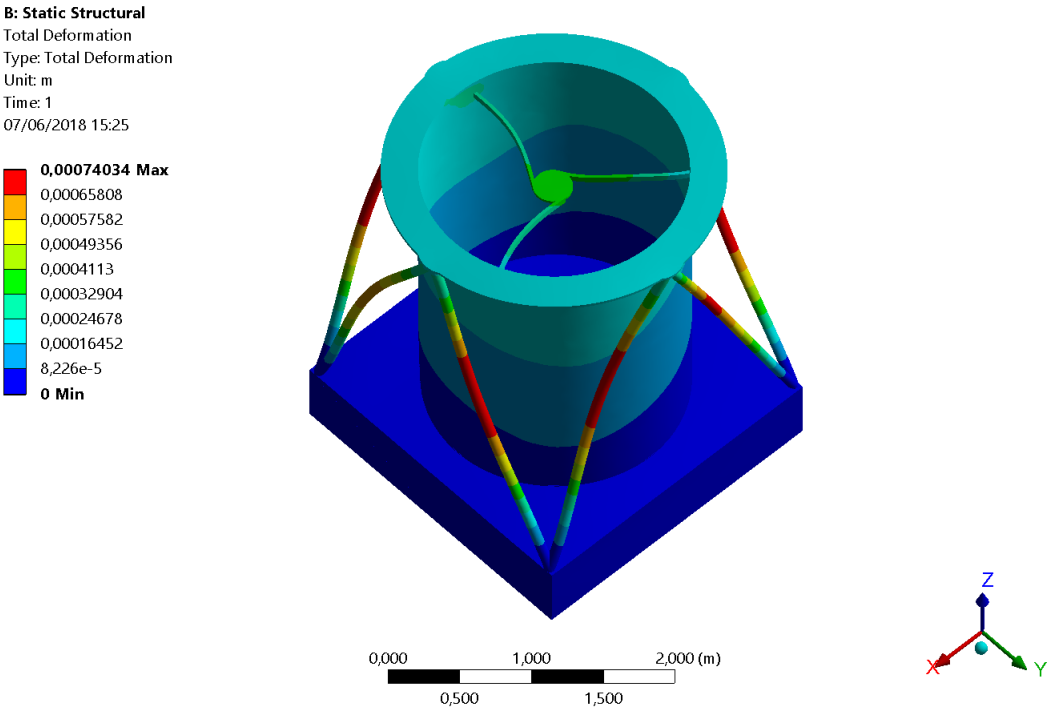

Figure 2.45: Total deformation

Modal analysis

Another important analysis which should be done is the modal one.
Zwicky's modal frequencies shall be higher than the frequencies of the launcher, in order to avoid mutual damages. These frequencies can be found in the launcher's manual. For the launcher selected in this mission (Ariane 6), frequencies higher than 6 Hz for the lateral and 20 Hz for the longitudinal are needed.
Also for the modal analysis the payload is fixed at the base.
The results from ANSYS software fit the requirements with large margins.
Only the modes that involve a conspicuous part of the mass are considered. The first mode is lateral and is above 93 Hz, while the first longitudinal mode is at about 201 Hz.

Frequency [Hz]	Direction
93.741	Lateral
201.33	Longitudinal

Table 2.19: Modal Frequencies

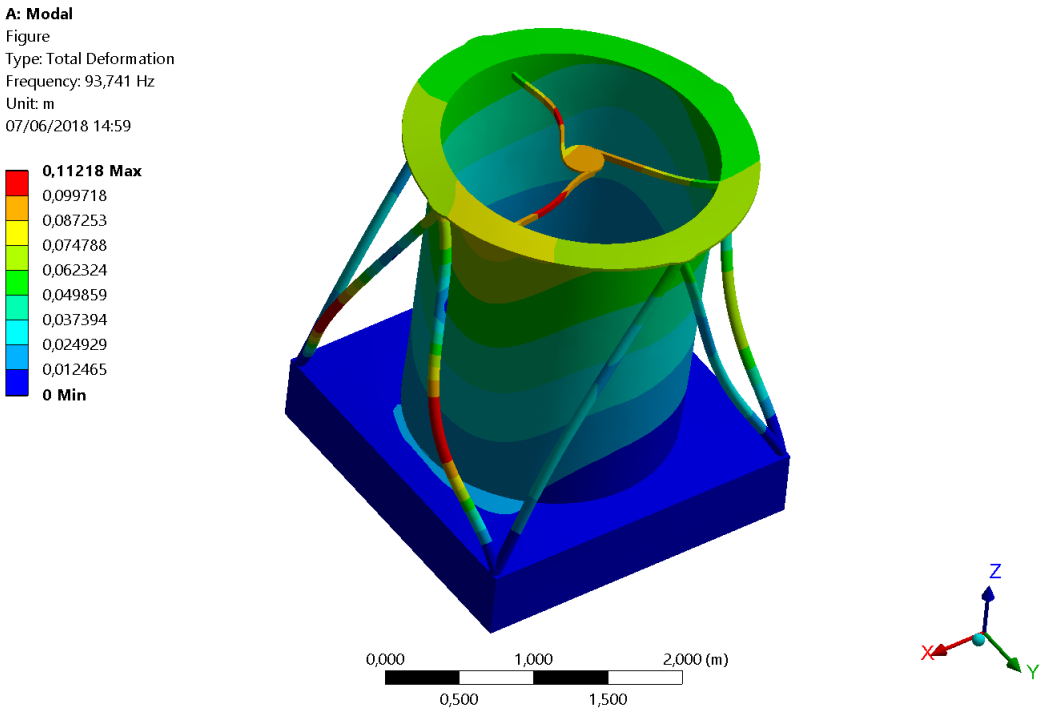

Figure 2.46: First lateral mode

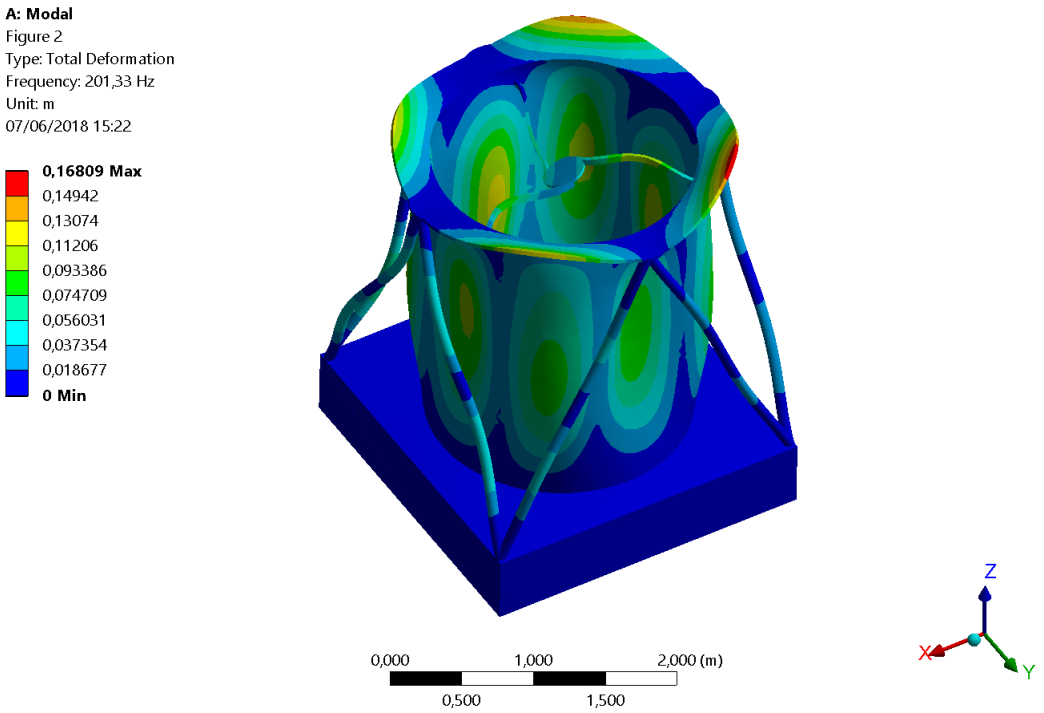

Figure 2.47: First longitudinal mode

2.3.4 CCD Unit

The selected CCD unit for Zwicky is the Teledyne CCD231-84, a summary of its properties are reported in the table 2.20.

Operating Temperature	160 K to 185 K
Radiation Hardness	N.P.A.
Power Supply	N.P.A
Power Dissipation	0.0011 W
Interfaces	Pin Grid Array (PGA)
Bit Depht	16 bit (black and white)

Table 2.20: CCD231-84

2.3.5 Spectrometer

The spectrometer selected for Zwicky has a custom design, since none was available on the market.
The preliminary properties needed to perform the sizing of Zwicky are reported in the table 2.21

Operating Temperature	223 K to 323 K
Radiation Hardness	N.P.A.
Power Supply	N.P.A
Power Dissipation	0.5 mW
Interfaces	LVDS
Bit Depht	16 bit

Table 2.21: Custom Spectrometer

2.3.6 Payload Data Handling

Data Processing Unit

The BAE Systems RAD 5545 SpaceVPX has been selected.
The RAD 5545 is a 64-bit quad-core PowerPC rad-hard System-on-Chip (SoC) capable of a 3.7 GFLOPS throughtput.
It provides up to 16 SpaceWire links, so it can be easily connected with other components of the system.
The operating system running on top of the SoC will be the WindRiver VxWorks OS, which has been widely used for space applications, offers support for the Power PC architecture, and has real-time capabilities, needed for any kind of space applications which requires strict timings.
The DPU shall interface with the SPU to select the acquisition source (CCD detector, NIR detector or both) and to select the operating mode of the SPU in real-time. In the table 2.22 are reported the properties of the RAD 5545 SoC:

Operating Temperature	218 K to 398 K
Size	6U - 220 × 30.48 mm
Radiation Hardness	Total ionizing dose: 100 krad (Si) ECC correction Latch-up immune
Power Supply	0.95 V +/- 5 percent core 1.5 or 1.8 V +/- 5 percent SerDes and double data rate (DDR) I/O 1.8 V, 2.5 V, and/or 3.3 V I/O (user programmable)
Power Dissipation	17.7 W at 95 °C
Interfaces	Four serial RapidIO ports across 16 lanes; up to 5 Gbaud/lane 16 SpaceWire links with embedded router Four I2C interfaces Serial peripheral interface (SPI) 32-bit parallel PCI Two dual UARTs (four simple or two advanced)
Memory	Dual DDR2/3 DRAM interfaces with interleaving NAND flash controller SRAM/EEPROM controller

Table 2.22: RAD 5545 SpaceVPX

Science Processing Unit

The BAE System RAD 5510 SpaceVPX has been selected.
The RAD 5510 is a single-core PowerPC rad-hard System-on-Chip (SoC), capable of a 0.9 GFLOPS throughput, and is equipped with the SpaceWire connector, so it can be connected with the other components of the system.
It provides both I2C and SPI I/O interfaces, so it can be easily connected with the instrument's readout electronics.
The operating system running on top of the SoC will be the WindRiver VxWorks OS, which has been widely used for space applications, offers support for the Power PC architecture, and has real-time capabilities, needed for any kind of space applications which requires strict timings.
In the table 2.23 are reported the properties of the RAD 5510 SoC:

Operating Temperature	218 K to 398 K
Size	6U - 220 × 30.48 mm
Radiation Hardness	Total ionizing dose: 100 krad (Si) ECC correction Latch-up immune
Power Supply	0.95 V +/- 5 percent core 1.5 or 1.8 V +/- 5 percent SerDes and double data rate (DDR) I/O 1.8 V, 2.5 V, and/or 3.3 V I/O (user programmable)
Power Dissipation	17.7 W at 95 °C
Interfaces	Four serial RapidIO ports across 16 lanes; up to 5 Gbaud/lane 16 SpaceWire links with embedded router Four I2C interfaces Serial peripheral interface (SPI) 32-bit parallel PCI Two dual UARTs (four simple or two advanced)
Memory	Dual DDR2/3 DRAM interfaces with interleaving NAND flash controller SRAM/EEPROM controller

Table 2.23: RAD 5510 SpaceVPX

Each SPU will be also responsible of constantly monitoring the health status of Zwicky's instruments and reporting them to the DPU.

Compressors

Image compression is an highly resource requiring task, but it is also needed for Zwicky, due to the very huge amount of data produced per day, especially from the CCDs array, so compression is strictly necessary.
Since the compression algorithm, which were briefly introduced in section 2.2.6, are the standard recommended by the CCSDS, those will be the ones implemented on Zwicky data handling subsystem.
Usually SW implementation of compression algorithms requires longer processing times and above all requires more power since the CPU has to run near its maximum frequency due to the heavy workload caused by the compression task, as outlined in [15], so an HW implementation will be used.

For what concerns image compression, the ESA CCSDS Wavelet Image COMpression (CWICOM) will be used, which implements the wavelet-based image compression which is the compression algorithm recommended in [23] for lossless science related image compression.
The CWICOM has an highly optimized internal architecture that allows performing lossless and lossy image compression at a very high data rate (up to 60 Mpixels/s). The CWICOM is implemented on a matrix of ATMEL ATC18RHA Application Specific Integrated Circuit (ASIC).
The properties of the CWICOM are reported in the table 2.24:

Operating Temperature	218 K to 398 K
Radiation Hardness	Total ionizing dose: 100 krad (Si) Latch-up immune
Operating Voltages	1.8 V for core and 3.3 V or 2.5 V for I/O's
Power Dissipation	100 mW/Mpix/s max (5 W - 6 W for 60 Mpix/s)
Interface	Ad-hoc implemented in FPGA

Table 2.24: CWICOM

For what concerns source data which comes from the spectrometer, the ESA Payload Rice Data Compressor (PRDC) will be used.
The PRDC implements the Rice algorithm for lossless data compression, which is the compression algorithm recommended in [22] for lossles data compression for science source data. The properties of the PRDC are reported in the table 2.25:

Operating Temperature	218 K to 398 K
Radiation Hardness	Total ionizing dose: 30 krad (Si) Latch-up immune
Operating Voltages	3 V
Power Dissipation	900 mW
Interface	Ad-hoc implemented in FPGA

Table 2.25: PRDC

Payload Mechanism Control Unit

The optics is equipped with a servomotor and a linear actuator, in addition, monitoring of the telescope tube is needed in order to detect possible deformations of the tube itself which will irredeemably damage the optics itself.
Since the tasks demanded to the Payload Mechanism Control Unit are not computationally intensive, a simple micro-controller can be used. The ATMEL AVR ATmegaS128 has been selected, and its properties are reported in the table 2.26:

Operating Temperature	218 K to 398 K
Radiation Hardness	Total ionizing dose: 30 krad (Si) Latch-up immune
Operating Voltages	3 V
Power Dissipation	300 mW
Interfaces	I2c SPI

Table 2.26: ATmegaS128

This choice let us to save some power and reduce the burden related to the development of the software due to the fact that the ATmega128 is a very popular micro-controller and the ATMmegaS128 is the space-compliant version of the very same hardware.

Storage Unit

The selected NAND FLASH unit is produced by 3D Plus and is currently available on the market.
It features a 60 krad total ionizing dose, 10 years data retention and a 200 mW power consumption.
Zwicky should use sox modules of 128 GB, in order to met the requirement on the data budget outlined in section 3.3.
Further documentation about the storage unit can be requested to 3D Plus if necessary.

2.3.7 Power Control and Distribution Unit

The Magellan Power Control Unit is the core of Zwicky power management.
Is capable of interfacing with solar arrays, batteries and the spacecraft power bus.
Can provide every component with the amount of power required and with the correct voltage and current.
It is a single unit capable of providing up to 300 W peak power and provides a total ionizing dose up of 50 krad (Si).
A complete list of all its properties can be found at [27].

2.3.8 Thermal Control Subsystem

The Thermal Control Subsystem is responsible of keeping all the components within their operative temperature ranges, which are reported in table 2.27.
This vital task must be carried out during the entire life of the mission, until the decommisionig phase.

COMPONENT	Temperature Range K
Telescope Structure	200 - 423
Service module	200 - 423
Mirrors	5 - 1500
Actuator (Micro3)	228 - 358
Actuator(SLL12)	228 - 358
CCDs Array (CCD231)	160 - 185
Spectrometers Array	223 - 323
CCDs Readout Electronics	153 - 323
Spectrometers Readout Electronics	153 - 323
DPU (RAD 5545)	218 - 398
DPU (RAD 5545) (Redundant)	218 - 398
SPU (CCDs)	218 - 398
SPU (Spectrometers)	218 - 398
SPU (Redundant)	218 - 398
Compressor (CWICOM)	218 - 398
Compressor (PRDC)	218 - 398
PMCU (ATMegaS128)	218 - 398
PMCU (Redundant)	218 - 398
NAND Flash	218 - 398
NAND Flash (Redundant)	218 - 398
Power Control Unit (Magellan)	243 - 333

Table 2.27: Temperature Ranges

The Thermal Control Subsystem (TCS) must face all the environmental heat fluxes coming from the region of the space Zwicky is orbiting into. Another source of heat is represented by the internal power dissipation coming from the on-board electronics.
As it operates in space, all the surfaces of Zwicky that are directly in contact with the external environment will radiate with different magnitudes towards deep space, depending on their temperatures and the optical property of the materials they are covered with.
An hypothesis that has been considered for the thermal modeling is that the telescope's tube shall always be shielded from the sun by a S/C solar panel. This assumption, however, constrains the portion of the celestial sphere that the telescope can observe to the area around the intersection between the celestial sphere and the plain perpendicular to the Sun-Telescope line. This is considered to be acceptable, as over 6 months the telescope is capable of covering all the celestial sphere, it just constrains the observation of specific objects to a specific time interval.

The designed thermal control subsystem is composed by the Multy-Layer Insulator (MLI)

covering the telescope tube and the instrument module, and 2 radiators.
The use of MLI is necessary, in order to reduce the influence that variable external heat fluxes have on the temperature of the internal components. Moreover the MLI around the tube is necessary in order to avoid temperature gradients which would lead to misalignment on the optics.
The main radiator has an area of $0.94\,m^2$ and is installed on one lateral face of the instrument module. It shall be connected to the various electronic components through heat pipes. As the CCD must be kept in a specific narrow temperature range, a smaller radiator dedicated to its cooling is needed. It is placed within the main radiator and shall have an area of $0.06\,m^2$. The CCD shall also be insulated from the supporting structure, in order to avoid conductive heat exchange.
Radiators shall be kept always facing the deep space.
A representation of the MLI and the radiators can be seen in figure 2.48.

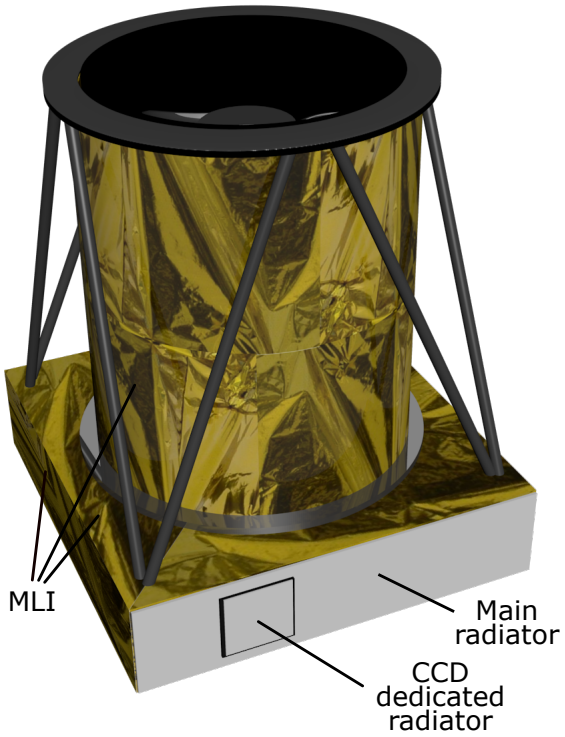

Figure 2.48: Thermal subsystem representation

In order to perform the modeling and the simulation of the TCS, Simscape has been used.
The thermal analysis focuses on the two extreme cases, one in which the total incoming heat flux is at its maximum (hot case), and on in which it is at int minimum (cold case). In the hot case, the internal heat generation has been considered as the maximum power the PDU could provide. On the contrary, for the cold case, the internal heat generation has been considered as half the maximum power the PDU could distribute.
For what concerns the CCD package, it dissipates 0.56 W when it is functioning. In the hot case it is considered to be turned on, while for the cold case, it is considered to be turned off.
The back of the S/C solar panel has been modeled as a radiating source with a constant

temperature of 300 K.
The albedo heat flow rate has been modeled as:

$$Q_{albedo} = 0.35 \cdot Q_{sun} \cdot A \cdot \epsilon$$

where Q_{sun} is the heat flux of the sun, equal to 1420 W/m^2, A is the area of the face exposed to the albedo and ϵ is the emissivity. The heat flow rate coming from the earth as been modeled as:

$$Q_{earth} = Q_i \cdot \frac{R_{Earth}}{R_{S/C}} \cdot A \cdot \epsilon$$

where Q_i is the energy flux at the Earth's surface, considered to be 271 Wm^2, A is the face exposed to the Earth radiation and ϵ is the emissivity.
The analysis does not take into account the heat exchanged with the S/C, as its functioning temperature range is not available at this stage. The table 2.28 summarizes the heat fluxes considered in the two cases.

Hot case	**Cold case**
Maximum heat dissipation from electronics	Minimum heat dissipation from electronics
CCD heat dissipation	No CCD heat dissipation
Irradiation from back of solar panel	Irradiation from back of solar panel
Albedo at perigee	Earth infrared radiation at apogee
Earth infrared radiation at perigee	

Table 2.28: Hot and cold cases incoming heat fluxes considered

To perform the thermal analysis, a multiple nodes approach has been followed: optics structure, service modules, electronics, CCD and the radiators are considered as thermal point masses. The electronic rack is mounted inside the service module and it exchanges heat via conduction with the latter.
Electronics is directly connected through an heat pipe to the main radiator; the CCD is also connected through an heat pipe to its radiator. The deep space has been be modeled as a thermal sink at 3 K.

The result of the thermal analysis are summarized in table 2.29 and in figure 2.49.

Node	**Cold case**	**Hot case**
Right	241.3	288.5
Back	241.4	288.6
Left	241.4	288.6
Front	241.4	288.6
Tube	241.3	288.6
Bottom	241.4	288.6
Electronics	241.4	288.8
CCD	160.7	180.9

Table 2.29: Thermal analysis results

As planned, all the devices are well within their operative temperature ranges.

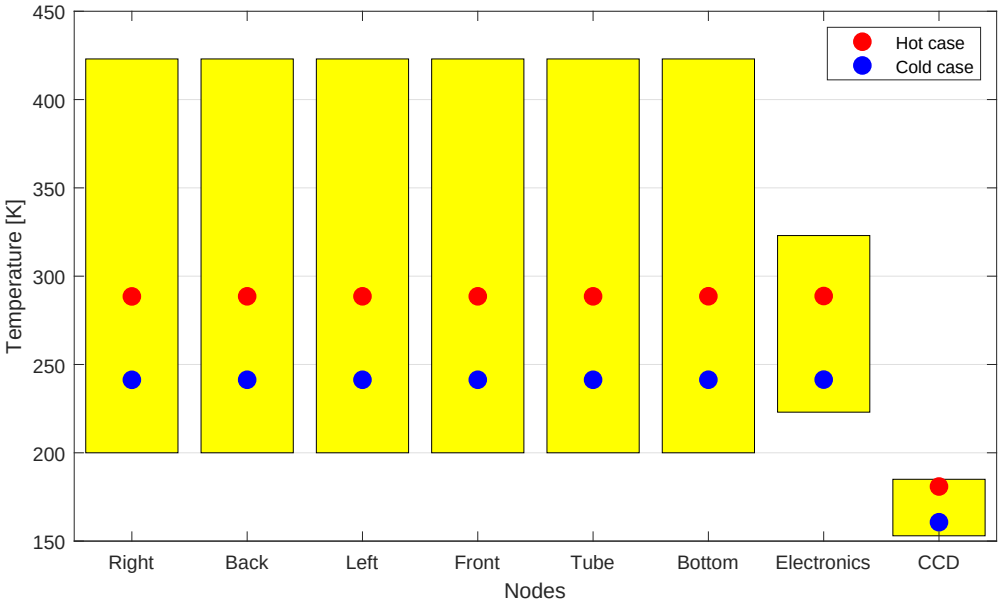

Figure 2.49: Temperature ranges and thermal analysis results

2.3.9 Components Shielding

Total Ionizing Dose

The ionizing radiation can cause degradation and functional failures in Zwicky devices. From the radiation environment analysis previously performed, it is possible to measure the radiation affecting the S/C.
In the following table is reported the total ionizing dose admissible for each component:

COMPONENT	Total Ionizing Dose [krad (Si)]
Actuator (Micro3)	N.A.
Actuator(SLL12)	N.A.
CCDs Array (CCD231)	-
Spectrometers Array	-
CCDs Readout Electronics	N.A.
Spectrometers Readout Electronics	N.A.
DPU (RAD 5545)	100
DPU (RAD 5545) (Redundant)	100
SPU (CCDs)	100
SPU (Spectrometers)	100
SPU (Redundant)	100
Compressor (CWICOM)	100
Compressor (PRDC)	30
PMCU (ATMegaS128)	30
PMCU (Redundant)	30
NAND Flash	60
NAND Flash (Redundant)	60
Power Control Unit (Magellan)	50

Table 2.30: Total Ionizing Dose

As it can be seen from 2.16, a minimum thickness of 12 mm between Zwicky's worst rad-hard component and the external environment is needed. As outilned in section 2.3.3, the thickness of the service module skin is 5 mm, so, as consequence, a 7 mm shielding is needed all over the electronics rack, in order to be safe from radiations.

2.4 Description of how the system works in each mission phase

2.4.1 Mission Phases Description

Launch Preparation

Once the assembly of Zwicky has been completed inside a clean room and after the transportation to the dedicated facility, Zwicky is mounted on the launcher's adapter, then it is placed inside the selected launcher's fairing. Pre-launch testing must be performed to ensure the correct fit inside the launcher and to check the correct behaviour of Zwicky's components.

Launch and early orbit phase

During the launcher lift-off, Zwicky shall be completely turned off. Zwicky shall withstand the maximum acceleration and the vibrations generated during the launch phase, whitout undergoing any kind of damage or loss of functionality.

Once the S/C is in orbit, ZWKICY's PCU and TCS are on, while the PDHS is set in idle, waiting for the "I'M ALIVE" message sent by the S/C to the ground segment.

In-orbit Commissioning

Once the orbit insertion is completed, the PDHS is fully active and performs a first check-up of all the subsystems.

Nominal Operations

Depending on the mission phase, Zwicky can be in one of the operative modes outlined in section 2.4.3

Spacecraft Disposal

Zwicky will be operative until it's EOL, when it will be dismissed through the decommissioning operation of the entire S/C, in accordance with the international rules for space debris mitigation.

2.4.2 Technology Readiness Level

The technology readiness level of each component has been assessed and reported in table 2.31. The technology related to the spectrometer results to be the less mature and consequently the most critical.

Subsystem	TRL
Optics	8
CCD	8 - 9
Spectrometer	5 - 6
Payload Data Handling	8 - 9
Power Bus	8 - 9
TCS	8 - 9

Table 2.31: Technology Readiness Level

2.4.3 Operative Modes

Zwicky can provide up to five different operational configurations in order to have a granular control of the power delivery to all its subsystems and to have a precise behaviour of the data handling unit in the different phases of the mission, according to the position on the orbit.
Those operative modes are:

- Acquiring Mode (A-MODE)
- Transmission mode (T-MODE)
- Stand-By Mode (SB-MODE)
- Safe Mode (SF-MODE)
- Commissioning Mode (C-MODE)

In the table 2.32 it is shown which subsystems are ON or OFF depending on the operative mode:

MODE	**Detection**	**PDHS**	**TCS**	**PCU**
A-MODE	ON	ON	ON	ON
T-MODE	OFF	ON	ON	ON
SB-MODE	OFF	IDLE	ON	ON
SF-MODE	OFF	IDLE	ON	ON
C-MODE	OFF/ON	OFF/ON	OFF/ ON	ON

Table 2.32: Operative Modes

Commisioning Mode

The commisioning mode is the first mode that shall be activated.
As it can be seen from table 2.32, detection subsystem, payload data handling subsystem and thermal control subsystem undergo a complete checkup through ON/OFF cycles.
The power control unit must be ON during the whole commisioning mode.
This mode is crucial to perform preliminary check-ups on the hardware and on the software, in order to detect any kind of bug.
The commissioning mode must also be activated after the safe mode, in order to perform a check up after the eventual problem that switched the payload into the safe mode.
From commissioning mode, either safe mode or stand-by mode can be activeted.
Commissioning mode can be activated only from safe mode.

Stand-By Mode

The stand-by mode can be seen as the link between the commissioning mode and the acquiring mode or between the commissioning mode and the transmission mode.
During the stand-by mode, the detection subsystem is OFF, and the payload data handling subsystem is in idle, waiting for commands. While in stand-by mode, either safe mode, acquiring

mode or transmission mode can be activated.
Stand-by mode can be activated by all other modes.

Acquiring Mode

The acquiring mode may be seen as the most power demanding mode, where all subsystem of the payload are switched ON and are performing their tasks. In fact this mode is designed to perform acquisition from both the detectors.
During this mode, the PDHS is also performing the data processing of the acquired data, and stores them into the NAND Flash unit.
From acquiring mode, safe mode and stand-by mode can be reached.
Acquiring mode can be reached only through stand-by mode.

Transmission Mode

During the transmission mode the detection subsystem is switched OFF and the PDHS is not performing data processing.
The data collected and processed by the payload are sent to the S/C OBDH to be transmitted to the ground segment.
From transmission mode either safe mode or stand-by mode can be activated.
Transmission mode can be reached only through stand-by mode.

Safe Mode

The safe mode is activated whenever required from the S/C or whenever the PDHS detect overheating of some component, HW failures or SW failures.
During the safe mode the PDHS is in idle, waiting for commands.
Being the emergency mode, it must be reached by all other modes in every situation.
Depending on the reason safe mode was activated for, either commisioning mode or stand-by mode can be activated after safe mode.

Chapter 3

Assessment of the performances

3.1 Mass Budget

Zwicky's mass budget is obtained considering each mass of each component. The following table reports Zwicky's mass budget and its relative margin:

COMPONENT	Nominal Mass [kg]	Mass (% Margin) [kg]
Service Module	951.55	1631.19 (+10%)
Telescope Structure	785,08	612.95 (+10%)
Primary Mirror	156.7	180.2 (+15%)
Secondary Mirror	1.8	2.07 (+15%)
Tertiary Mirror	4.5	5.18 (+15%)
First Reflecting Mirror	3.6	4.14 (15%)
Second Reflecting Mirror	4.2	4.83 (+15%)
Dichroic Mirror	2.5	2.88 (+15%)
Moving Mirror	1.9	2.19 (+15%)
Actuator (Micro3)	3.2	3.84 (+20%)
Actuator(SLL12)	0.103	0.124 (+20%)
CCDs Array	0,500	0.65 (+30%)
Spectrometers Array	0,128	0.17 (+30%)
CCDs Readout Electronics	0.5	0.675 (+35%)
Spectrometers Readout Electronics	0.5	0.675 (+35%)
DPU (RAD 5545)	1.5	2.02 (+35%)
DPU (RAD 5545) (Redundant)	1.5	2.02 (+35%)
SPU (CCDs)	1.5	2.02 (+35%)
SPU (Spectrometers)	1.5	2.02 (+35%)
SPU (Redundant)	1.5	2.02 (+35%)
Compressor (CWICOM)	0.8	1.08 (+35%)
Compressor (PRDC)	0.8	1.08 (+35%)
PMCU (ATMegaS128)	0.6	0.81 (+35%)
PMCU (Redundant)	0.6	0.81 (+35%)
NAND Flash	0.6	0.81 (+35%)
NAND Flash (Redundant)	0.6	0.81 (+35%)
Power Control Unit (Magellan)	27	29.7 (+10%)
Cables & Mountings	18	25.2 (+40%)
TOTAL	1937.26	2187.94

Table 3.1: Mass Budget

3.2 Power Budget

Zwicky is not self-sufficient in terms of power, so all the power required by each component will be provided by the S/C through the Magellan Power Control Unit, which is capable of interfacing between the solar array, battery (if they are present on the S/C) and S/C power bus. Since the Magellan Power Control Unit can be scaled according to the mission requirements, it is necessary to identify a list of every component needing a power supply and the amount of power required. In the following table both informations are expressed, taking into account margins for worst case scenario:

COMPONENT	Nominal Power [W]	Power (% Margin) [W]
Actuator (Micro3)	6	8.10 (+35%)
Actuator (SLL12)	2	3.35 (+45%)
CCDs Array	0.060	0.0810 (+35%)
Spectrometers Array	0.0132	0.0178 (+35%)
CCDs Readout Electronics	0.5	0.675 (+35%)
Spectrometers Readout Electronics	0.5	0.675 (+35%)
DPU (RAD 5545)	17.7	25.67 (+45%)
DPU (RAD 5545) (Redundant)	17.7	25.67 (+45%)
SPU (CCDs)	17.7	25.67 (+45%)
SPU (Spectrometers)	17.7	25.67 (+45%)
SPU (Redundant)	17.7	25.67 (+45%)
Compressor (CWICOM)	96	110.4 (+15%)
Compressor (PRDC)	1	1.35 (+35%)
PMCU (ATMegaS128)	0.5	0.675 (+35%)
PMCU (Redundant)	0.5	0.675 (+35%)
NAND Flash	0.6	0.81 (+35%)
NAND Flash (Redundant)	0.6	0.81 (+35%)
Power Control Unit (Magellan)	20	24 (+20%)
TOTAL	216.77	279.97

Table 3.2: Power Budget

Power enlisted for each component has to be intended as peak power required, while for the majority of time during nominal operations the average power required will be lower.

3.3 Data Budget

Every time an acquisition sequence is succesfully completed, the responsible SPU generates a data file named with a code which contains the following informations:

- acquisition sequence
- acquisition time
- acquisition coordinates

The weight of each generated file will depend on the detector which is performing the acqusition. In the fore-after are reported the computations.

CCD Array

The size of each frame captured by a single CCD can be computed as follows.
The first thing to be computed is the total number of pixels generated by an acquisition of the detector:

$$\text{Number of Pixel} = 4100 \times 4100 = 16\,810\,000\,\text{pixel}$$

$$\text{Total bits of Data} = 16810000 \times 16 = 268\,960\,000\,\text{bit}$$

where 16 is the bit depth of the detector. To get a practical number in terms of a more common measurement unit this value has to be divided by 8 to have the size in *bytes* and by 2048 to have the size in terms of *megabytes*:

$$\frac{268960000}{8 \times 2048} = 32.06\,\text{MB}$$

The total size of a frame then can be obtained by multiplying this number by the total number of detectors:

$$32.08\,\text{MB} \times 16 = 513\,\text{MB}$$

Spectrometers Array

The size of each frame captured by a single spectrometer can be computed as follows.
The first thing to be computed is the total number of pixels generated by an acquisition of the detector:

$$\text{Number of Pixel} = 2286\,\text{pixel}$$

$$\text{Total bit of Data} = 2286 \times 16 \times 33778 = 1\,235\,464\,128\,\text{bit}$$

where 16 is the bit depth of the detector and 33778 is the maximum number of acquisition of a single FOV. To get a practical number in terms of a more common measurement unit this value has to be divided by 8 to have the size in *bytes* and by 2048 to have the size in terms of *megabytes*:

$$\frac{1235464128}{8 \times 2048} = 147.27\,\text{MB}$$

The total size of a frame can then be obtained by multiplying this number by the total number of detectors:

$$147.27\,\text{MB} \times 12 = 1767.35\,\text{MB}$$

To evaluate the total amount of data generated per orbital period, it is crucial to know the amount of frames per day that should be acquired and stored.
Considering a worst case scenario where a frame every 35 minutes is captured for 44 hours, the total amount of data generated by Zwicky during the acquisition mode is given by:

COMPONENT	Data
CCD Array	39 501 MB/orbital period
Spectrometer Array	136 085.95 MB/orbital period
TOTAL	175.586 GB/orbital period

Table 3.3: Data Budget

So, taking into account a safety margin of 100%, the amount of on-board non-volatile memory required by Zwicky is 351 GB.

Data Transfer

Without any compression, considering that the communication window lasts 4 hours, the amount of data per hour which shall be sent to Earth is about 43.9 GB, which is quite a large number. In order to reduce the amount of data sent to Earth, the compression factor reported in table 3.4 are applied:

COMPONENT	Uncompressed	Compressed
CCD Array	39 501 MB	4937.62 MB (C.R. = 8)
Spectrometer Array	136 085.95 MB	13 608.59 MB (C.R. = 10)
TOTAL	175.586 GB	18.5 GB

Table 3.4: Compression

Then, in 4 hours, 4.6 GB per hour have to be sent.
So, the final requirement for the S/C telecommunication subsystem is that it shall be able to send at least 10.22 Mbit/s.

Chapter 4

Identification of risk areas

4.1 Optics

Nothing can mitigate a possible failure of the optics, although a failure of the optics is very unlikely to happen. Damages in fact can be due to unexpected launch loads, impact with a space debris or possible non-uniform deformation of the telescope tube caused by overheating, which could lead to misalignment or damages to the mirrors.
All this factor has been considered during the design phase.

4.2 CCD Array

The only risk concerning the CCDs array is the failure of one of the grid composing the detector. For this reason instead of a single huge CCD, an array composed by multiple CCDs has been selected. In this case a failure of one component results in the loss of only a portion of the FOV and not in the complete incapability to acquire images in the visible spectrum.
Thanks to a study conducted by ESA (European Space Agency) the main sources of the failure of the CCDs have been identified and are listed below:

- Oxide defect / Bulk defect
- Hot carrier
- Dielectric breakdown / Instability
- Interconnections / Stressed Induced Void
- Particle contamination
- Coating pollution
- Disbonding (delamination)
- Oxide charging

4.3 Spectrometer Array

A possible risk concerning the spectrometer is the failure of one of the detectors composing the array. For this reason, instead of a single huge detector, an array composed of multiple detectors has been selected. In the array case, if the spectrometer looses a detector, only a line

of the FOV is lost and the information that Zwicky can still acquire is enough to accomplish the requirements.
Other risk related to this system are the moving mirror and the trail on which the array of detectors is moving. The moving mirror is rotating thanks to the rotary actuator and in case of its failure the possibility of operating spectral acquisition is lost. For this reason a secondary actuator is built in the system to provide the needed redundancy.
For the trail a redundancy similar to the rotary actuator cannot be implemented. In case of failure of this element acquisition can still be done thanks to the movement of the telescope, that can provide the linear movement needed to scan all the FOV. The movement needed is really small so that the amount of propellant used should be low. However the precision obtained is not as high as the one granted by the linear actuator. Also the acquisition time increases due to the fact that, while the spacecraft is moving, the CCDs can't do any acquisition and so, infrared and visible detector can only work separately and not simultaneously like in the nominal working case.

4.4 Structure

The main risks for the failure of the structure are due to unexpected loads during the launch phase or due to the impact with debris in the orbiting phase.
It is not convenient to prevent this problems with a structure more robust than it already is.

4.5 Thermal Control Subsystem

The thermal control subsystem is a passive device, so it's very unlikely to undergo any kind of malfunctioning.
S/C's ADCS failures however, can lead to a wrong orientation of the S/C on its orbit. If the radiators comes to face a body which emits a significant amount of heat flux, a surplus of heat can enter the system, causing unexpected behaviour.

4.6 Payload Data Handling Subsystem

A possible risk area for what concerns the payload data handling subsystem could be the sudden loss of functionality of some of the computers of the PDHS or of a memory stick.
To mitigate the risk, as it can be seen from section 2.2.7, a redundant storage unit is placed in parallel to the default one.
For what concerns the computers, a second quiescent DPU (RAD 5545) is present and is activated if the first DPU undergoes HW failure or if a system upgrade is needed on the first DPU.
For the very same reasons, a third quiescent SPU is placed in parallel to the default SPUs. The backup SPU is a RAD 5545 and not a RAD 5510 (which are the default SPUs), in order to provide enough computational power in the case of failure of both the default SPUs.

Chapter 5

Conclusions

Zwicky satisfies all technical requirements without any evidence of non-compliance and its general specifications, about mass and power, are in line with the values requested by customers.

Considering the main purpose of Zwicky, it is possible to state that the payload is able to take pictures and acquire spectral data of far galaxies for a wide range of time and that it is able to compress the obtained data, sending them to the ground station in a restricted range of time.